

## RESEARCH ARTICLE

# FOXO1 cooperates with C/EBP $\delta$ and ATF4 to regulate skeletal muscle atrophy transcriptional program during fasting

Mamoru Oyabu<sup>1</sup> | Kaho Takigawa<sup>1</sup> | Sako Mizutani<sup>1</sup> | Yukino Hatazawa<sup>1</sup> |  
 Mariko Fujita<sup>1</sup> | Yuto Ohira<sup>1</sup> | Takumi Sugimoto<sup>1</sup> | Osamu Suzuki<sup>2</sup>  |  
 Kyoichiro Tsuchiya<sup>3</sup> | Takayoshi Suganami<sup>4</sup>  | Yoshihiro Ogawa<sup>5</sup>  |  
 Kengo Ishihara<sup>6</sup>  | Shinji Miura<sup>7</sup>  | Yasutomi Kamei<sup>1</sup> 

<sup>1</sup>Laboratory of Molecular Nutrition, Graduate School of Life and Environmental Sciences, Kyoto Prefectural University, Kyoto, Japan

<sup>2</sup>Laboratory of Animal Models for Human Diseases, National Institutes of Biomedical Innovation, Health and Nutrition, Osaka, Japan

<sup>3</sup>Third Department of Internal Medicine, Interdisciplinary Graduate School of Medicine and Engineering, University of Yamanashi, Yamanashi, Japan

<sup>4</sup>Department of Molecular Medicine and Metabolism, Research Institute of Environmental Medicine, Nagoya University, Nagoya, Japan

<sup>5</sup>Department of Medicine and Bioregulatory Science, Graduate School of Medical Sciences, Kyushu University, Fukuoka, Japan

<sup>6</sup>Department of Food Science and Human Nutrition, Faculty of Agriculture, Ryukoku University, Shiga, Japan

<sup>7</sup>Graduate School of Nutritional and Environmental Sciences, University of Shizuoka, Shizuoka, Japan

## Correspondence

Yasutomi Kamei, Laboratory of Molecular Nutrition, Graduate School of Life and Environmental Science, Kyoto Prefectural University, Kyoto 606-8522, Japan.  
 Email: kamei@kpu.ac.jp

## Funding information

Ministry of Education, Culture, Sports, Science and Technology (MEXT), Grant/Award Number: 19H04058 and 21K19728; The Fuji Foundation for Protein Research; The Tojuro Iijima Foundation for Food Science and Technology

## Abstract

Catabolic conditions, such as starvation, inactivity, and cancer cachexia, induce Forkhead box O (FOXO) transcription factor(s) expression and severe muscle atrophy via the induction of ubiquitin–proteasome system-mediated muscle proteolysis, resulting in frailty and poor quality of life. Although FOXOs are clearly essential for the induction of muscle atrophy, it is unclear whether there are other factors involved in the FOXO-mediated transcriptional regulation. As such, we identified FOXO–CCAAT/enhancer-binding protein  $\delta$  (C/EBP $\delta$ ) signaling pathway as a novel proteolytic pathway. By comparing the gene expression profiles of FOXO1-transgenic (gain-of-function model) and FOXO1,3a,4<sup>-/-</sup> (loss-of-function model) mice, we identified several novel FOXO1-target genes in skeletal muscle including *Redd1*, *Sestrin1*, *Castor2*, *Chac1*, *Depp1*, *Lat3*, as well as C/EBP $\delta$ . During starvation, C/EBP $\delta$  abundance was increased in a FOXOs-dependent manner. Notably, knockdown of C/EBP $\delta$  prevented the induction of the ubiquitin–proteasome system and decrease of myofibers in FOXO1-activated

**Abbreviations:** 4-OHT, 4-hydroxytamoxifen; 4EBP1, eukaryotic translation initiation factor 4E-binding protein 1; ATF4, activating transcription factor 4; Atrogin-1, muscle atrophy F-box; C/EBP $\delta$ , CCAAT/enhancer-binding protein  $\delta$ ; DBE, Daf-16 binding element; FOXO, Forkhead box O; FOXO1, 3a,4<sup>-/-</sup>, skeletal muscle-specific FOXO1,3a,4 triple knockout; FOXO1-Tg, skeletal muscle-specific FOXO1-transgenic; KEGG, Kyoto Encyclopedia of Genes and Genomes; mTOR, mechanistic target of rapamycin; MyHC, myosin heavy chain; S6K, ribosomal S6 kinase; SUNSET, surface sensing of translation; UPS, ubiquitin–proteasome system; WT, wild type.

myotubes. Conversely, C/EBP $\delta$  overexpression in primary myotubes induced myotube atrophy. Furthermore, we demonstrated that FOXO1 enhances the promoter activity of target genes in cooperation with C/EBP $\delta$  and ATF4. This research comprehensively identifies novel FOXO1 target genes in skeletal muscle and clarifies the pathophysiological role of FOXO1, a master regulator of skeletal muscle atrophy.

#### KEYWORDS

ATF4, C/EBP $\delta$ , fasting, FOXO1, skeletal muscle atrophy

## 1 | INTRODUCTION

The largest organ in the human body is the skeletal muscle, accounting for approximately 40% of the body weight. Excessive muscle proteolysis promotes loss of muscle mass and strength, which has been commonly recognized in detrimental catabolic conditions, such as starvation, disuse-induced muscle atrophy, and cancer cachexia. Evidence has suggested that the prevention of muscle atrophy is critical for preventing increased morbidity and mortality, as well as improving health and quality of life.<sup>1,2</sup> Therefore, it is essential that we fully understand the molecular mechanisms regulating muscle atrophy.

Skeletal muscle mass is rigorously controlled by the rate of protein degradation and synthesis.<sup>3–5</sup> The critical mediators of proteolysis are Forkhead box O (FOXO) family transcription factors,<sup>6</sup> which induce ubiquitin–proteasome system (UPS)-mediated protein degradation via the induction of muscle-specific E3 ligases, such as Atrogin1/MAFbx and MuRF1/Trim63.<sup>4,7</sup> Moreover, FOXOs activate autophagy as another proteolytic system.<sup>8,9</sup> Studies using FOXO genetically-modified mice have unveiled FOXO transcription factors as central mediators for both UPS- and autophagy-mediated muscle proteolysis in diverse pathological conditions, such as starvation and denervation,<sup>10,11</sup> inactivity,<sup>12,13</sup> diabetes mellitus,<sup>14</sup> and chronic kidney disease.<sup>15</sup> Despite these advances in understanding proteolytic signaling pathways that facilitate muscle atrophy, it is still unclear whether there are critical factors that mediate transcriptional regulation by FOXOs. The UPS-mediated muscle proteolysis is also enhanced by CCAAT/enhancer-binding protein  $\delta$  (C/EBP $\delta$ ), which is required for the upregulation of Atrogin1/MAFbx and Myostatin (a negative regulator of muscle mass) expression and promotes skeletal muscle atrophy in vivo.<sup>16,17</sup> The use of C/EBP $\delta$  knockout mice has illustrated the key role of C/EBP $\delta$  in promoting muscle atrophy, which is based on the observation that these mice are resistant to muscle loss and have improved survival in chronic kidney disease.<sup>17</sup> Although previous studies

demonstrated that C/EBP $\alpha$  and C/EBP $\beta$ , other members of the C/EBP family, coordinately function with FOXO1 in the liver<sup>18</sup> and other cells,<sup>19,20</sup> studies are yet to determine the relationship between FOXOs and C/EBP $\delta$ . Another essential transcription factor that promotes muscle atrophy is activating transcription factor 4 (ATF4), whose overexpression is sufficient to reduce muscle fiber size in vivo.<sup>21,22</sup>

We previously observed that FOXO1 transgenic mice (FOXO1-Tg) with skeletal muscle-specific overexpression of FOXO1 demonstrated significant muscle atrophy; FOXO1 was found to be an important factor in causing muscle atrophy in vivo.<sup>23</sup> Our laboratory and other groups have revealed that FOXOs induce the expression of muscle atrophy-related genes, such as *PDK4* (regulator of cellular energetic metabolism),<sup>24</sup> *Cathepsin L* (lysosomal proteolytic enzyme),<sup>25</sup> *Gadd45a* (regulator of muscle atrophy),<sup>23</sup> and *4EBP1* (translation inhibitor).<sup>26–30</sup> These observations suggest that FOXOs function as master regulators of muscle atrophy, which prompted us to investigate the target genes of FOXOs in skeletal muscle. Although previous pioneering studies have uncovered the target genes and functions of FOXOs in skeletal muscle using either murine gain- or loss-of-function experimental models,<sup>10–12,14,23,31</sup> studies are yet to report on genetic and molecular pathways involved in FOXO-mediated transcriptional regulation using both of the genetically modified mice. Therefore, analyses using both gain- and loss-of-function mouse models of FOXOs have the potential to facilitate the discovery of a new causal molecular mechanism and FOXO target genes for muscle atrophy.

In this study, we comprehensively identified novel FOXO1-target genes in skeletal muscle using both FOXO1-Tg mice (gain-of-function model) and FOXO1,3a,4<sup>-/-</sup> mice (loss-of-function model). Using FOXO1-activated cultured myotubes, we uncovered a novel intracellular signaling pathway from FOXO1 to the UPS, with C/EBP $\delta$  as the intermediary link between FOXO1 and the UPS-mediated muscle proteolysis. Our results also demonstrated that FOXO-dependent induction of C/EBP $\delta$  and

ATF4 coordinately enhanced the transcriptional program with FOXOs.

## 2 | MATERIALS AND EXPERIMENTAL PROCEDURES

### 2.1 | Animal protocols

To generate the FOXO1,3a,4<sup>-/-</sup> mice devoid of skeletal muscle-specific FOXO1, FOXO3a, and FOXO4 expression, plasmids for Cre recombinase driven by a human  $\alpha$ -skeletal actin promoter were microinjected into fertilized eggs from FOXO1,3a,4-floxed mice [FOXO1,3a,4<sup>fl/fl</sup> mice (denoted as WT mice)] in which LoxP sequences were inserted into the FOXO1, FOXO3a, and FOXO4 genes (Exon2, Exon2, and Exon1, respectively) (Figure S1A).<sup>32,33</sup> Cre transgene detection PCR was performed using the following primers: 5'-CGCCGCATAACCAGTGAAAC-3' and 5'-ATGTCCAATTTACTGACCG-3'. Skeletal muscle-specific FOXO1 transgenic mice (FOXO1-Tg) were prepared as previously described.<sup>23</sup> Briefly, the expression of the human FOXO1 gene was driven by the human  $\alpha$ -skeletal actin promoter in skeletal muscle (C57BL/6 background). The mice were housed at a constant temperature of 24°C under artificial light (light/dark cycle of 12 h), with *ad libitum* access to food (CE-2, CLEA, Japan) and water. Animal experiments were conducted with strict observance to Kyoto Prefecture University Animal Research Committee guidelines. Male mice were used for all experiments. The study protocol was approved by the Committee (no. KPU260407, review board: Dr. Yasuhiro Tsukamoto). Surgical procedures were performed after a cervical dislocation or under sodium pentobarbital anesthesia to minimize suffering.

### 2.2 | Fasting of mice

FOXO1,3a,4<sup>-/-</sup> (2–4-months old) and age-matched WT mice were fasted in individual cages for 24 or 48 h, whereas control mice were fed *ad libitum*. After fasting, skeletal muscles (gastrocnemius, quadriceps, tibialis anterior, extensor digitorum longus, soleus, and plantaris muscles) were collected and rapidly frozen in liquid nitrogen for subsequent analyses. Blood glucose levels of fed and 24 h-fasted FOXO1,3a,4<sup>-/-</sup> (2–4-months old) and age-matched WT mice were measured with Glu-test Sensor and Glu-test Every glucose meter (Sanwa Kagaku Kenkyusho, Japan) using blood collected from mouse tails ( $n = 6$ ). Fasting experiments were replicated three times.

### 2.3 | Histological analysis

The tibialis anterior muscles from fed and 48 h-fasted FOXO1,3a,4<sup>-/-</sup> (2-months old) and age-matched WT mice were fixed in 10% neutral buffered formalin ( $n = 3-5$ ). Immunostaining was performed using an antibody against laminin (rabbit polyclonal antibody, 1:200, ab11575, Abcam). The tibialis anterior muscles from the FOXO1-Tg (3–5-months old) and age-matched control mice were fixed in liquid nitrogen-cooled isopentane ( $n = 3$ ). Hematoxylin and eosin were used to stain prepared transverse serial sections. Immuno-stained images were analyzed using BZ-X800 Analyzer software (Keyence, Osaka, Japan) to measure the whole muscle cross-sectional area. Muscle cross-sectional area from the FOXO1-Tg and control mice was determined as the minimum Feret diameter from at least 380 muscle fibers using ImageJ 1.52q software (National Institutes of Health, USA, <https://imagej.nih.gov/ij>).

### 2.4 | Glucose and insulin tolerance tests

FOXO1,3a,4<sup>-/-</sup> mice (3–4-months old) and age-matched WT mice ( $n = 7$ ) were subjected to glucose tolerance test and insulin tolerance test as previously performed.<sup>23</sup> Briefly, for the insulin tolerance test, insulin (0.75 mU/g of body weight) was intraperitoneally administered to fed mice; whereas for the glucose tolerance test, D-glucose (1 mg/g of body weight) was administered orally to mice after fasting overnight.

### 2.5 | Measurements of energy expenditure and oxygen consumption

FOXO1,3a,4<sup>-/-</sup> mice (2–3-months old) and age-matched WT mice were placed in individual metabolic chambers coupled to a mass spectrometer (ARCO-2000; ARCO System, Japan) with *ad libitum* access to food (CE2, CLEA Japan) and water ( $n = 8$ ). Oxygen consumption ( $VO_2$ ), respiratory exchange ratio (the ratio of the volume of  $CO_2$  produced to the volume of  $O_2$  consumed), carbohydrate oxidation, lipid oxidation, and energy expenditure were determined using a gas analysis system as previously described.<sup>34,35</sup> Respiratory exchange ratio values approaching 0.7 are indicative of exclusive fat utilization, whereas exclusive carbohydrate utilization is represented by values close to 1.0. At 72 h after commencement of measurements, mice were subjected to a 30 h fast, and subsequently re-fed with soy protein-based high-fat diets (40% of calories from sucrose, 40% from fat, and 20% from protein). High-fat diets (4.6 kcal/g, soy protein 200 g, sucrose 396 g, lard

155.1 g, cellulose 50 g, calcium carbonate 5.5 g, L-cystine 3 g, soybean oil 25 g, dicalcium phosphate 13 g, mineral mix S10026 10 g, potassium citrate monohydrate 16.5 g, vitamin mix V10001 10 g, and choline bitartrate 2 g) were purchased from Research Diets (NJ).<sup>35</sup>

## 2.6 | Western blot analysis

Snap-frozen skeletal muscles (gastrocnemius and quadriceps) were homogenized using Tissue Lyser II (Qiagen, Hilden, Germany) at 30 Hz for 2 min per cycle (three cycles) in an ice-cold RIPA Lysis Buffer cocktail (#20-188, Merck KGaA, Darmstadt, Germany) supplemented with 1% protease inhibitor cocktail (P-8340, Sigma, St. Louis, MO), 1 mM sodium orthovanadate, and 1 mM PMSF (phenylmethylsulfonyl fluoride). Centrifugation at 15 000× *g* for 15 min at 4°C was performed for supernatant retrieval. Preparation of cell protein lysates involved incubation in supplemented ice-cold RIPA Lysis Buffer cocktail (#20-188, Merck) for 10–15 min. A 27 G syringe needle (0.40 × 19 mm) was used to better homogenize the cell lysates. Subsequent protein concentration was determined using the BCA protein assay kit (23227, Pierce, Rockford, IL). Another aliquot was mixed with Sample Buffer Solution without 2-mercaptoethanol (30567-12, Nacalai Tesque, Japan) supplemented with dithiothreitol (D9779, Sigma) at a final concentration of 40–50 mM and heated at 97°C for 5 min.

An equal amount of protein (20, 13, and 6 µg for tissues, C2C12 cells, and primary myotubes, respectively) from each sample was subjected to sodium dodecyl sulfate-polyacrylamide gel electrophoresis using 7.5%, 10%, 15%, or 5%–20% polyacrylamide precast gels (e-PAGEL, ATTO Co., Tokyo, Japan) and transferred to a nitrocellulose membrane (Bio-Rad Laboratories, Hercules, CA). Blocking was done using either 5% skim milk or 5% bovine serum albumin (BSA) for 1 h at room temperature. Immunoblot was performed using primary antibodies against FOXO1 (rabbit monoclonal antibody, 1:1000 #2880, Cell Signaling Technology, Danvers, MA), FOXO3a (rabbit polyclonal antibody, 1:1000, GTX100277, GeneTex, Irvine, CA), C/EBPδ (rabbit polyclonal antibody, 1:1000, #2318, Cell Signaling Technology), Atrogin1 (mouse monoclonal antibody, 1:500, sc-166806, Santa Cruz Biotechnology, Dallas, TX), Ubiquitin (rabbit polyclonal antibody, 1:1000, #3933, Cell Signaling Technology), p-mTOR (Ser2448) (rabbit monoclonal antibody, 1:1000, #5536, Cell Signaling Technology), mTOR (rabbit monoclonal antibody, 1:1000, #2983, Cell Signaling Technology), p-4EBP1 (Thr37/46) (rabbit monoclonal antibody, 1:1000, #2855, Cell Signaling Technology), 4EBP1 (rabbit monoclonal antibody, 1:1000, #9644, Cell Signaling Technology), p-S6K

(Thr389) (rabbit monoclonal antibody, 1:1000, #9234, Cell Signaling Technology), S6K (rabbit monoclonal antibody, 1:1000, #2708, Cell Signaling Technology), p-S6 ribosomal protein (Ser235/236) (rabbit monoclonal antibody, 1:1000, #4857, Cell Signaling Technology), S6 ribosomal protein (rabbit monoclonal antibody, 1:1000, #2217, Cell Signaling Technology), p-eIF2α (Ser51) (rabbit monoclonal antibody, 1:1000, #ab32157, Abcam), eIF2α (rabbit polyclonal antibody, 1:1000, #9722, Cell Signaling Technology), and myosin heavy chain (MyHC) (mouse monoclonal antibody, 1:500, MF-20, Developmental Studies Hybridoma Bank, Iowa City, IA) overnight at 4°C. Membranes were subsequently treated with horseradish peroxidase-conjugated secondary antibodies (1:2000, NA934V, GE Healthcare, Buckinghamshire, UK, or 1:2000, NA931V, GE Healthcare) for 1 h at room temperature. Blot detection was performed using the ECL Prime Western Blotting Detection Reagent (RPN2232, GE Healthcare) and ChemiDoc XRS<sup>+</sup> Imaging System (Bio-Rad) was used for image capture. Image Lab software (Bio-Rad) was used to quantify signal intensities.

## 2.7 | RNA extraction, reverse transcription, and qPCR

TRIzol solution (Thermo Fisher Scientific Inc., Tokyo, Japan) was used for total RNA extraction from cells and tissues. The total RNA (500 ng) served as a template for cDNA synthesis using ReverTra Ace quantitative PCR (qPCR) RT MasterMix with gDNA remover (Toyobo, Tokyo, Japan). mRNA expression was measured on a CFX Connect Real-Time PCR Detection System (Bio-Rad) using Thunderbird SYBR qPCR Mix or Thunderbird Next SYBR qPCR Mix (Toyobo). Data analysis was conducted using the  $\Delta\Delta C_t$  method. All data obtained were normalized with 36B4, 18S, or GAPDH expression. In each experiment, stable 36B4, 18S, or GAPDH expression was used as an internal control. All primers were validated by examining the obtained melt curves and peaks, which enabled to determine the target specificity of the PCR reaction. The primers used are shown in Supporting Information Table S2.

## 2.8 | Microarray analysis

RNA was isolated from skeletal muscle (quadriceps) of fed and 24 h-fasted FOXO1,3a,4<sup>-/-</sup> mice (8–9 weeks old) and age-matched WT mice (*n* = 4). Extracted RNA purification was performed using an RNeasy Mini kit (Qiagen). The purity of the RNA was determined by measuring ultraviolet absorbance at 260 and 280 nm,

which confirmed that there was no contamination of proteins. RNA was electrophoresed in 1.2% denaturing agarose gel, and the patterns of ribosomes 28S and 18S were observed, confirming that all samples had similar migration patterns, suggesting total RNA was not degraded (Figure S1B). Using the Low Input Quick Amp labeling kit, samples were labeled with cyanine 3-CTP (Agilent Technologies, Inc., Santa Clara, CA) and hybridized to the Agilent whole-mouse genome (8 × 60 K) microarray. Hybridized microarray slide scanning was done with the Agilent Microarray Scanner (G2565CA, Agilent Technologies). Signal interpretation and data analysis were performed as recommended by the manufacturer's instructions.

## 2.9 | Functional enrichment analysis of microarray data

The GO biological process enrichment and KEGG pathway analysis were conducted using the comprehensive bioinformatics resource functional annotation tool DAVID v6.8.<sup>36</sup> Submission of a list of 381 genes with decreased expression profiles (FDR < 0.05) in skeletal muscle of 24 h-fasted FOXO1,3a,4<sup>-/-</sup> versus 24 h-fasted WT mice revealed significant overrepresentation of the GO biological process terms and KEGG pathway.

## 2.10 | Construction of protein–protein interaction networks and identification of hub genes

Protein–protein interaction networks were constructed using the STRING database,<sup>37</sup> and the protein–protein interaction networks were further modeled using Cytoscape 3.8.2 software.<sup>38</sup> Gene clusters were constructed using the ClusterViz plugin. The color of nodes was mapped to log<sub>2</sub> fold change values and circle size was mapped to the degree of genes. The 381 gene symbols representing lowly expressed genes (FDR < 0.05) in skeletal muscle of 24 h-fasted FOXO1,3a,4<sup>-/-</sup> versus 24 h-fasted WT mice were submitted to the STRING database.

## 2.11 | Amino acid analysis

Snap-frozen skeletal muscles (quadriceps) from fed and 24 h-fasted FOXO1,3a,4<sup>-/-</sup> and WT mice were homogenized using Tissue Lyser II (Qiagen) at 30 Hz for 7 min in 2.5% sulfosalicylic acid solution (*n* = 6). This was followed by supernatant separation through centrifugation (15 000× *g* for 10 min at 4°C) and high-performance liquid

chromatography measurements of amino acids (SRL, Tokyo, Japan).

## 2.12 | C2C12 cell culture

C2C12 mouse myoblasts (Riken Cell Bank, Tsukuba, Japan) with stable expression of FOXO1-ER fusion proteins were prepared as reported previously.<sup>25,39</sup> Briefly, C2C12 cells were stably transfected with either empty pBabe retrovirus vector or the pBabe retrovirus vector expressing fusion proteins, containing a constitutively active form of human FOXO1. Three Akt phosphorylation sites (Thr<sup>24</sup>, Ser<sup>256</sup>, and Ser<sup>319</sup>) were replaced with alanine (FOXO1[3A]) in-frame with a modified tamoxifen-specific version of the murine ER ligand-binding domain. Puromycin was used for cell selection. FOXO1-ER fusion proteins were restricted to the cytoplasmic fraction until activation by 4-hydroxytamoxifen (4-OHT), which prompted nuclear translocation and FOXO1 moiety-mediated transcription.<sup>39</sup> C2C12 myoblast(s) growth medium consisted of Dulbecco's Modified Eagle's Medium (DMEM) supplemented with 10% fetal bovine serum (FBS) and 1% penicillin–streptomycin. The C2C12 myoblasts (passage 17–18) were plated in 12-well plates at a density of 1 × 10<sup>5</sup> cells/well until the cells reached 80% confluence. After reaching 80% confluence, the cells were treated with either 4-OHT (1 μM) or dimethyl sulfoxide (DMSO, vehicle) for 24 h before RNA extraction. To induce C2C12 myotube differentiation, the C2C12 myoblasts (passage 18–23) were cultured in a differentiation medium containing DMEM supplemented with 2% horse serum and 1% penicillin–streptomycin and plated in 6, 12, and 24-well plates at a density of 1 × 10<sup>5</sup> cells/ml for up to 7 days.

## 2.13 | RNAi in C2C12 cells expressing FOXO1(3A)-ER

For the RNAi experiments in C2C12 myoblasts and myotubes expressing FOXO1-ER fusion protein, the C2C12 myoblasts and myotubes (1 × 10<sup>5</sup> cells/ml) were cultured in 6, 12, and 24-well plates. After C2C12 myoblasts reached 80%–90% confluence or C2C12 myotubes differentiated for 5 days, siRNA was transfected with Lipofectamine RNAiMax (13778–150, Invitrogen, Carlsbad, CA) at a final concentration of 30 nM in accordance with the manufacturer's instructions. Six hours after transfection, 4-OHT (1 μM) was administered in the cells to translocate the FOXO1-ER fusion protein into the nucleus. Two siRNA for C/EBPδ (MISSION siC/EBPδ [SASI\_Mm01\_00093692] and MISSION siC/EBPδ [SASI\_Mm01\_00093693]) and

ATF4 (MISSION siATF4 [SASI\_Mm02\_00316863] and MISSION siATF4 [SASI\_Mm02\_00316864]) and control siRNA (MISSION siRNA Universal Negative Control #1) were purchased from Sigma–Aldrich (St. Louis, MO). siRNA sequences are shown in Supporting Information Table S3.

## 2.14 | Immunofluorescent staining

For immunofluorescence analysis, C2C12 myoblasts stably expressing FOXO1-ER ( $1 \times 10^5$  cells/ml) were differentiated for 5 days in 24-well plates, after which 4-OHT ( $1 \mu\text{M}$ ) was administered to the cells. At 24 or 48 h after 4-OHT treatment, C2C12 myotubes were washed with phosphate-buffered saline (PBS) containing 0.025% Tween20 (PBST), followed by fixation in 4% paraformaldehyde for 10 min. In the case of primary myotubes, satellite cell-derived myoblasts ( $1 \times 10^5$  cells/ml) were differentiated for 4 days in 24-well plates, after which primary myotubes were fixed 2% with paraformaldehyde in GlutaMAX™ DMEM (10569-010, Thermo Fisher Scientific) for 10 min. After PBST washing, cells were permeabilized and concomitantly blocked with 0.3% Triton X-100 in PBS supplemented with 10% goat serum for 20 min. Washed cells were then incubated with primary antibodies against MyHC (MF-20, Developmental Studies Hybridoma Bank, mouse monoclonal antibody, 1:50) in 1% BSA in PBS overnight at 4°C. This was followed by myotube incubation with the fluorescence-labeled secondary antibody (A11004, Life Technologies, Carlsbad, CA, 1:400) in 1% BSA in PBS for 1 h at room temperature. Several washing steps were followed, including three PBST washes, PBS containing 4,6-diamidino-2-phenylindole (DAPI) wash, followed by three PBST washes. Nuclei were counterstained with a mounting medium containing DAPI (0100-20, SouthernBiotech, Birmingham, AL). Image detection was performed using a fluorescent microscope (BZ-X800, Keyence) and analyzed using BZ-X800 Analyzer software (Keyence) to measure the fluorescence intensity and fluorescence-positive area. At least six locations per well were imaged, and average values were calculated. The myotube diameter was quantified from at least 240 fibers/condition from 4 independent wells.

## 2.15 | SUnSET assay

The surface sensing of translation (SUnSET) technique is a nonradioactive method to monitor and quantify global protein synthesis in mammalian cells.<sup>40</sup> Briefly, C2C12 myotubes were incubated at 37°C in a

differentiation medium containing  $1 \mu\text{M}$  puromycin (100552, MP Biomedicals, Solon, OH) for 30 min and then immediately washed with PBST, followed by fixation in 4% paraformaldehyde for 10 min. C2C12 myotubes were incubated with primary antibodies against puromycin (mouse monoclonal antibody, 1:2000, clone 12D10, MABE343, Merck) in 1% BSA in PBS overnight at 4°C. This was followed by incubation with fluorescence-labeled secondary antibody (1:400, A11004, Life technologies) in 1% BSA in PBS at room temperature for 1 h. Nuclei were counterstained with a mounting medium containing DAPI (0100-20, Southern Biotech). Images were detected through fluorescence microscopy (BZ-X800, Keyence).

## 2.16 | Immunoprecipitation of MyHC

For co-immunoprecipitation analysis, C2C12 myoblasts stably expressing FOXO1-ER were differentiated for 5 days in 100-mm dishes, after which DMSO or 4-OHT ( $1 \mu\text{M}$ ) was administered to the cells for 24 h with or without  $10 \mu\text{M}$  MG-132 (474790, Sigma), a proteasome inhibitor. Preparation of cell lysates involved incubation in ice-cold RIPA Lysis Buffer cocktail (Merck) supplemented with 1% protease inhibitor cocktail (Sigma), 1 mM sodium orthovanadate, and 1 mM PMSF for 10–15 min. A 22 G syringe needle ( $0.8 \times 32$  mm) was used to better homogenize the cell lysates. Centrifugation at  $10\,000 \times g$  for 10 min at 4°C was performed for supernatant retrieval. Cell lysates were precleared by adding  $1.0 \mu\text{g}$  of control mouse IgG (normal mouse IgG, #12-371, Merck), together with  $20 \mu\text{l}$  of resuspended protein A/G-agarose beads (sc-2003, Santa Cruz Biotechnology) for 30 min at 4°C. This was followed by centrifugation at  $1000 \times g$  for 5 min at 4°C for supernatant retrieval. Subsequent protein concentration was determined using BCA protein assay kit (Pierce) and then protein lysates were incubated with anti-MyHC antibody (mouse monoclonal antibody, MF-20, Developmental Studies Hybridoma Bank) for 1 h at 4°C. Prior to incubation, the aliquot of total cell lysates was stored at 4°C, separately. The immunoprecipitated complexes were bound to protein A/G beads for 2 h at 4°C on a rotator and then washed four times with a RIPA Lysis Buffer cocktail (Merck).

## 2.17 | Primary satellite cell

The extensor digitorum longus muscles were collected from 8-week-old C57BL/6J mice and digested in 0.2% Type I Collagenase (4197, Worthington, Freehold,

NJ) dissolved in GlutaMAX™ DMEM (Thermo Fisher Scientific) in a shaking incubator for 1 h 45 min. Satellite cells were harvested from isolated muscle fibers through Accutase (12679-54, Nacalai Tesque, Japan) treatment for 10 min. This was followed by culturing in the growth medium [DMEM glucose [–] (A14430-01, Thermo Fisher Scientific) supplemented with 30% FBS, 1% chicken-embryo extract (C3999, US Biological), 1% GlutaMAX (35050-061, Thermo Fisher Scientific), 1% penicillin-streptomycin, and 10 ng/ml basic fibroblast growth factor (450-33, PeproTech, Rocky Hill, NJ)] using 150-mm dishes coated with Matrigel (354230, BD Biosciences, San Diego, CA).

## 2.18 | Plasmid constructs: C/EBPδ, ATF4, and FOXO1 expression vectors

pcDNA 3.1(–) C/EBPδ plasmid (Plasmid #12559) was purchased from Addgene (Watertown, MA), and the cDNA sequence of C/EBPδ was amplified by PCR. The unique *Bam*HI and *Eco*RI sites were incorporated at the 5' and 3' ends of the sequences to simplify directional cloning into *Bam*HI and *Eco*RI sites in pCMX-vector. The pCMX-flag-C/EBPδ vectors were digested with *Eco*RI and *Hind*III and then the FLAG-tagged C/EBPδ was cloned into the pMX retroviral vector with a blunt end. Primer sequences are shown in Supporting Information Table S4. pCMV-driven FLAG-tagged murine ATF4 (pCMV-flag-ATF4) plasmid and pcDNA3.1 murine ATF4 cDNA (pcDNA3.1-ATF4) plasmid were prepared as previously described.<sup>41</sup> The pCAG-driven constitutively active form of human FOXO1 (caFOXO1) [pCAG-FOXO1(3A)] plasmid was prepared as previously described.<sup>25</sup> All plasmid constructs were confirmed by Fasmac sequencing service (Fasmac, Kanagawa, Japan).

## 2.19 | Transfection in satellite cell-derived myoblasts

The isolated satellite cell-derived myoblasts were plated in Matrigel-coated 12, and 24-well plates at a density of  $1 \times 10^5$  cells/ml for qRT-PCR analysis, and immunofluorescent staining, respectively. Satellite cell-derived myoblasts were then transfected with 0.8 μg of expression plasmids [pCMX-GFP, pCMX-C/EBPδ, pCMV-flag-ATF4, or pCAG-FOXO1(3A)] using Lipofectamine 2000 (11668-019, Invitrogen). Six hours after transfection, the myogenic differentiation was induced by replacing the medium with a differentiation medium (GlutaMAX™ DMEM supplemented with 5% horse serum and 1% penicillin-streptomycin) for 4 days.

## 2.20 | Stable expression of C/EBPδ

Plat-E cells, retrovirus packaging cells, were cultured in 100-mm dishes in DMEM supplemented with 10% FBS until 90%–100% confluence was attained. In C/EBPδ stable overexpression experiment, Plat-E cells were transfected with 6 μg of either the pMX-GFP retroviral vector or pMX-C/EBPδ retroviral vector using Lipofectamine 2000 (Invitrogen). Six hours after transfection, the medium was replaced with DMEM supplemented with 10% FBS. At 48 h after transfection, the viral supernatant collected from the cultured Plat-E cells was filtered through a 0.45-μm sterilization filter, and polybrene was added at a final concentration of 5 μg/ml. Satellite cells-derived myoblasts were then infected at a 1:1 ratio of viral supernatant and growth medium. The cells were selected twice with puromycin (3 μg/ml) to eliminate any uninfected cells. The infected satellite cells-derived myoblasts were plated in Matrigel-coated 6, 12, and 24-well plates at a density of  $1 \times 10^5$  cells/ml for western blotting, qRT-PCR, and immunofluorescent staining, respectively. After day 1, the cells were differentiated into myotubes in a differentiation medium (GlutaMAX™ DMEM supplemented with 5% horse serum and 1% penicillin-streptomycin).

## 2.21 | Cloning of mouse C/EBPδ, ATF4, Redd1, Sestrin1, Castor2, Chac1, Depp1, and Lat3 promoters

The pGL3-C/EBPδ, pGL3-ATF4, pGL3-Redd1, pGL3-Sestrin1, pGL3-Castor2, pGL3-Chac1, pGL3-Depp1, and pGL3-Lat3 plasmids containing the C/EBPδ, ATF4, Redd1, Sestrin1, Castor2, Chac1, Depp1, and Lat3 promoters, followed by the *luciferase* genes, respectively, were generated by cloning the PCR-amplified murine C/EBPδ, ATF4, Redd1, Sestrin1, Castor2, Chac1, Depp1, and Lat3 promoter fragments into pGL3-basic luciferase vectors (Promega). Genome DNA isolated from the skeletal muscle (gastrocnemius) of a C57BL/6J mouse was subjected to PCR to amplify the DNA fragments containing promoter region (C/EBPδ: –1933 to +243, ATF4: –1604 to +882, Redd1: –1907 to +221, Sestrin1: –1643 to +714, Castor2: –1997 to +172, Chac1: –2142 to +340, Depp1: –1706 to +274, and Lat3: –1406 to +365). The PCR-amplified fragments were subjected to the second PCR to generate the C/EBPδ, ATF4, Redd1, Sestrin1, Castor2, Chac1, Depp1, and Lat3 promoter fragments (C/EBPδ: –1500 to +25, ATF4: –1500 to +100, Redd1: –1500 to +100, Sestrin1: –1100 to +130, Castor2: –1900 to +100, Chac1: –2000 to +100, Depp1: –1500 to +100, and Lat3: –1000 to +90), in which the unique restriction enzyme recognition sites were incorporated at

the 5' and 3' ends of the sequences to simplify directional cloning into corresponding restriction enzyme recognition sites in pGL3-basic luciferase vectors (C/EBP $\delta$ : *NheI* and *HindIII*, ATF4: *XhoI* and *BglII*, Redd1: *XhoI* and *HindIII*, Sestrin1: *XhoI* and *HindIII*, Castor2: *XhoI* and *BglII*, Chac1: *HindIII* and *HindIII*, Depp1: *XhoI* and *HindIII*, and Lat3: *XhoI* and *BglII*); primer sequences are shown in Supporting Information Table S5. Sestrin1, Castor2, and Lat3 promoter fragments were inserted into p7Blue T-vectors (Merck) and subsequently subcloned into pGL3-basic luciferase vectors. All plasmid constructs were confirmed by the Fasmac sequencing service (Fasmac).

## 2.22 | HEK293T transfection and luciferase assay

HEK293T cells ( $2 \times 10^5$  cells/well) were plated in 12-well plates in DMEM supplemented with 10% FBS. After the cells reached 80%–90% confluence, luciferase reporter plasmids, containing promoter fragments (C/EBP $\delta$ , ATF4, Redd1, Sestrin1, Castor2, Chac1, Depp1, and Lat3) (0.8  $\mu$ g), expression plasmids [pCAG-FOXO1(3A), pCMX-C/EBP $\delta$ , and pcDNA3.1-ATF4: 0.2  $\mu$ g], pCMX-GFP (up to 0.8  $\mu$ g), and phRL-TK vector (25 ng, Promega Co., Madison, WI) as an internal control of transfection efficiency, were transfected into HEK293T cells using Lipofectamine 2000 (Invitrogen). Five hours after transfection, the medium was replaced with DMEM supplemented with 10% FBS. After 24 h, the cells were lysed in Reporter Lysis Buffer (Promega), followed by a single freeze-thaw cycle at  $-80^\circ\text{C}$ . Firefly and Renilla luciferase activities were assayed using the Dual-Glo Luciferase assay kit (Promega) and GloMax Navigator Microplate Luminometer (Promega). Final luciferase activity was calculated as the ratio of the firefly luciferase activity to the Renilla luciferase activity (internal control). Four wells per condition were assigned. All experiments were replicated at least twice using each luciferase gene plasmid.

## 2.23 | Statistical analysis

Student's two-tailed unpaired t-test was performed for comparisons between two groups only when their normality was confirmed. Comparisons of three or more study groups were performed using either one-way or two-way analysis of variance (ANOVA) followed by Tukey's *post hoc* test. Analysis of non-normally distributed data even when log-transformed involved the Kruskal–Wallis test followed by Dunn's *post hoc* test. Normality tests were adopted when the sample size was 5 or more. All statistical analyses were performed using the GraphPad Prism

9.1 software (GraphPad software, San Diego, CA) except for the microarray data analysis. Data were expressed as mean  $\pm$  SD.  $p < .05$  was considered statistically significant and classified as \* $p < .05$ , \*\* $p < .01$ , and \*\*\* $p < .001$ .

## 3 | RESULTS AND DISCUSSION

### 3.1 | Deletion of FOXO1,3a,4 induces muscle hypertrophy

In the previous report, we observed obvious muscle atrophy in FOXO1-Tg mice with overexpression of FOXO1 in skeletal muscle.<sup>23</sup> To assess whether the endogenous FOXO family functions as an essential regulator for atrophy, we generated skeletal muscle FOXO1,3a,4-triple-knockout mice (hereafter referred to as FOXO1,3a,4<sup>-/-</sup>), in which Cre recombinase was driven by human  $\alpha$ -skeletal actin promoter (Figure S1A). Successful knockout of FOXOs was confirmed through quantitative reverse transcription-PCR (qRT-PCR), which revealed a lack of *FOXO1*, *FOXO3a*, and *FOXO4* transcript expression in skeletal muscle only, but not in other tissues, including insulin-sensitive tissues (liver and white adipose tissue) (Figure S1C–E), and Cre recombinase was overexpressed specifically in skeletal muscle (Figure S1F). Therefore, successful generation of FOXO1,3a,4<sup>-/-</sup> mice was confirmed.

To examine the role of FOXOs in skeletal muscle during fasting, FOXO1,3a,4<sup>fl/fl</sup> mice (wild type, WT) and FOXO1,3a,4<sup>-/-</sup> mice were fasted. qRT-PCR analysis showed a significant increase of *FOXO1*, *FOXO3a*, and *FOXO4* transcripts in skeletal muscle of fasted WT mice, whereas the induction of FOXOs transcripts during fasting was completely suppressed in FOXO1,3a,4<sup>-/-</sup> muscle (Figure 1A). Western blot experiments revealed a marked increase in FOXO1 (but not FOXO3a) protein levels during fasting in WT mice, whereas the increase of FOXO1 protein levels was abolished in FOXO1,3a,4<sup>-/-</sup> mice (Figure 1B). Although body weight, liver weight, and adipose tissue mass were not discriminated between WT mice and FOXO1,3a,4<sup>-/-</sup> mice, larger skeletal muscle mass (quadriceps, extensor digitorum longus, soleus, and plantaris) was observed in FOXO1,3a,4<sup>-/-</sup> mice, indicating that deletion of FOXO1,3a,4 in skeletal muscle induces muscle hypertrophy (Figure S2A–C). Consistently, muscle fiber size (mean muscle cross-sectional area measured in tibialis anterior) of FOXO1,3a,4<sup>-/-</sup> mice seemed to be larger than WT mice, although the difference did not reach statistical significance (Figure S2D–F). Muscle fiber size was not significantly affected in 48 h-fasted WT mice compared with fed WT mice in this experiment possibly because of the short-term fasting (Figure S2D–F). Blood glucose levels decreased in both WT and FOXO1,3a,4<sup>-/-</sup> mice, reflective of fasting (Figure S3A). Moreover, when insulin tolerance

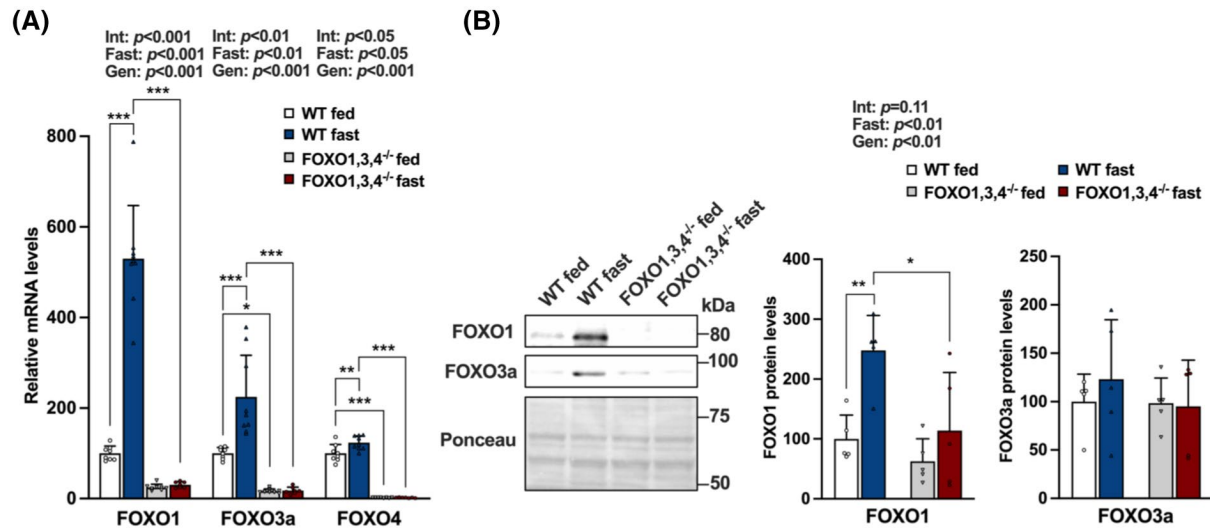


**FIGURE 1** FOXO1, 3a, 4 expression was abolished in FOXO1,3a,4<sup>-/-</sup> mice during fasting. (A) Quantitative RT-PCR of FOXO1, FOXO3a, and FOXO4 in the quadriceps of fed and 24 h-fasted FOXO1,3a,4<sup>-/-</sup> and FOXO1,3a,4<sup>fl/fl</sup> (denoted as WT in the figures) mice. Data were normalized to 36B4 expression and illustrated as values relative to the control mice (WT, fed) ( $n = 7-9$  mice per group). (B) Immunoblots and densitometric analysis of FOXO1 and FOXO3a protein levels in the gastrocnemius of fed and 24 h-fasted FOXO1,3a,4<sup>-/-</sup> and WT mice. Representative immunoblots were shown ( $n = 5$  mice per group). Values are mean  $\pm$  SD. \* $p < .05$ , \*\* $p < .01$ , and \*\*\* $p < .001$ . (A, B) Fasting effects (Fast), genotype effects (Gen), and interaction between fasting and genotype effects (Int) were analyzed by two-way ANOVA followed by Tukey's *post hoc* test

and glucose tolerance tests were performed, FOXO1,3a,4<sup>-/-</sup> mice demonstrated normal insulin sensitivity and glucose tolerance (Figure S3B,C). Consistently, the expression of hepatic FOXO1 and gluconeogenic genes [phosphoenolpyruvate carboxykinase (PEPCK) and glucose-6-phosphatase (G6Pase)] was maintained in the liver of FOXO1,3a,4<sup>-/-</sup> mice, suggesting that gluconeogenesis seemed to occur in the same way as WT mice under fasting conditions in FOXO1,3a,4<sup>-/-</sup> mice (Figure S3D,E). Furthermore, there was no difference in energy expenditure, oxygen consumption ( $VO_2$ ), and respiratory exchange ratio between WT mice and FOXO1,3a,4<sup>-/-</sup> mice under basal and fasting conditions, indicating that the increase in muscle mass in FOXO1,3a,4<sup>-/-</sup> mice did not affect whole-body energy expenditure (Figure S4).

### 3.2 | Overexpression of FOXO1 induces robust reduction of muscle fiber size

To confirm whether FOXO1 overexpression is sufficient for the reduction of muscle fiber size, we also measured muscle cross-sectional area in FOXO1-Tg mice. FOXO1-Tg mice had a significantly smaller muscle cross-sectional area than control mice as evaluated by hematoxylin and eosin staining. Moreover, consistent with the previous reports,<sup>23</sup> FOXO1-Tg mice demonstrated less muscle mass than control mice (Figure S5A-C). Taken together, based on the observation that FOXO1 overexpression was sufficient for the reduction

of muscle fiber size, we conclude that elevated FOXO1 level in skeletal muscle induces muscle atrophy *in vivo*.

### 3.3 | FOXOs increase C/EBP $\delta$ abundance and activate the UPS, and conversely decrease p-4EBP1/4EBP1 levels in skeletal muscle during fasting

Muscle fiber size is controlled by protein degradation and synthesis.<sup>5</sup> Thus, we evaluated the abundance of C/EBP $\delta$ , muscle-specific E3 ligase *Atrogin1* expression, and ubiquitinated protein levels as markers for protein degradation and mTORC1 activity as a marker for protein synthesis. The abundance of C/EBP $\delta$  protein and *Atrogin1* expression significantly increased in fasted WT muscle but were completely abolished in fasted FOXO1,3a,4<sup>-/-</sup> muscle (Figure 2A,B,D), indicating that FOXOs are responsible for the induction of C/EBP $\delta$  and UPS-mediated proteolysis during fasting. Consistently, total ubiquitinated protein levels, which are used as substrates for both proteasomal degradation and autophagy, tended to increase in fasted WT muscle but were completely abolished in fasted FOXO1,3a,4<sup>-/-</sup> muscle (Figure 2A,B).

We next assessed the mTORC1 activity, which promotes muscle hypertrophy and prevents muscle atrophy *in vivo*.<sup>30</sup> Thr37/46 phosphorylation of 4EBP1 relative to total 4EBP1 markedly increased in fed and fasted FOXO1,3a,4<sup>-/-</sup> mice compared to WT mice (Figure 2A,B). Conversely,

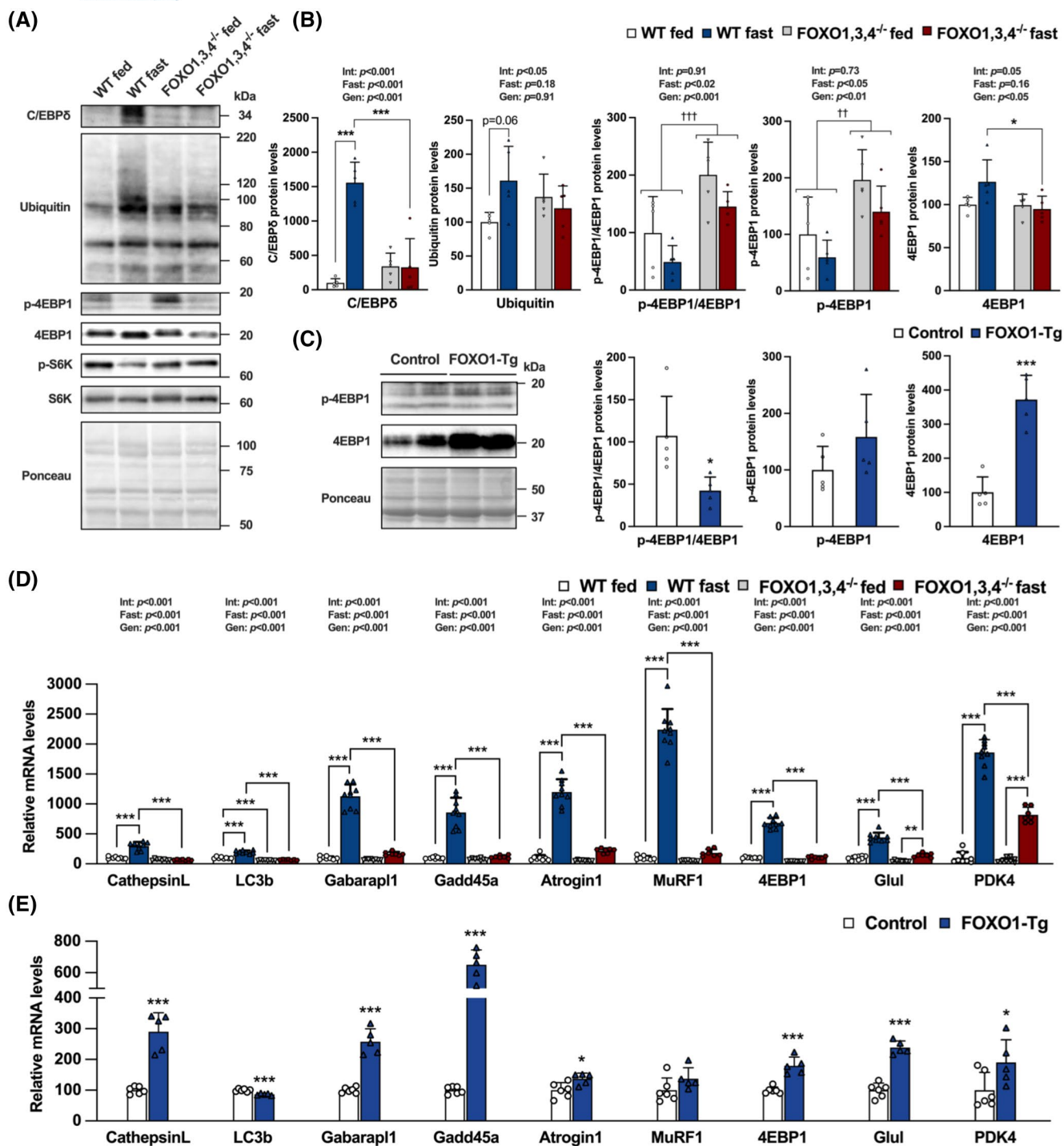
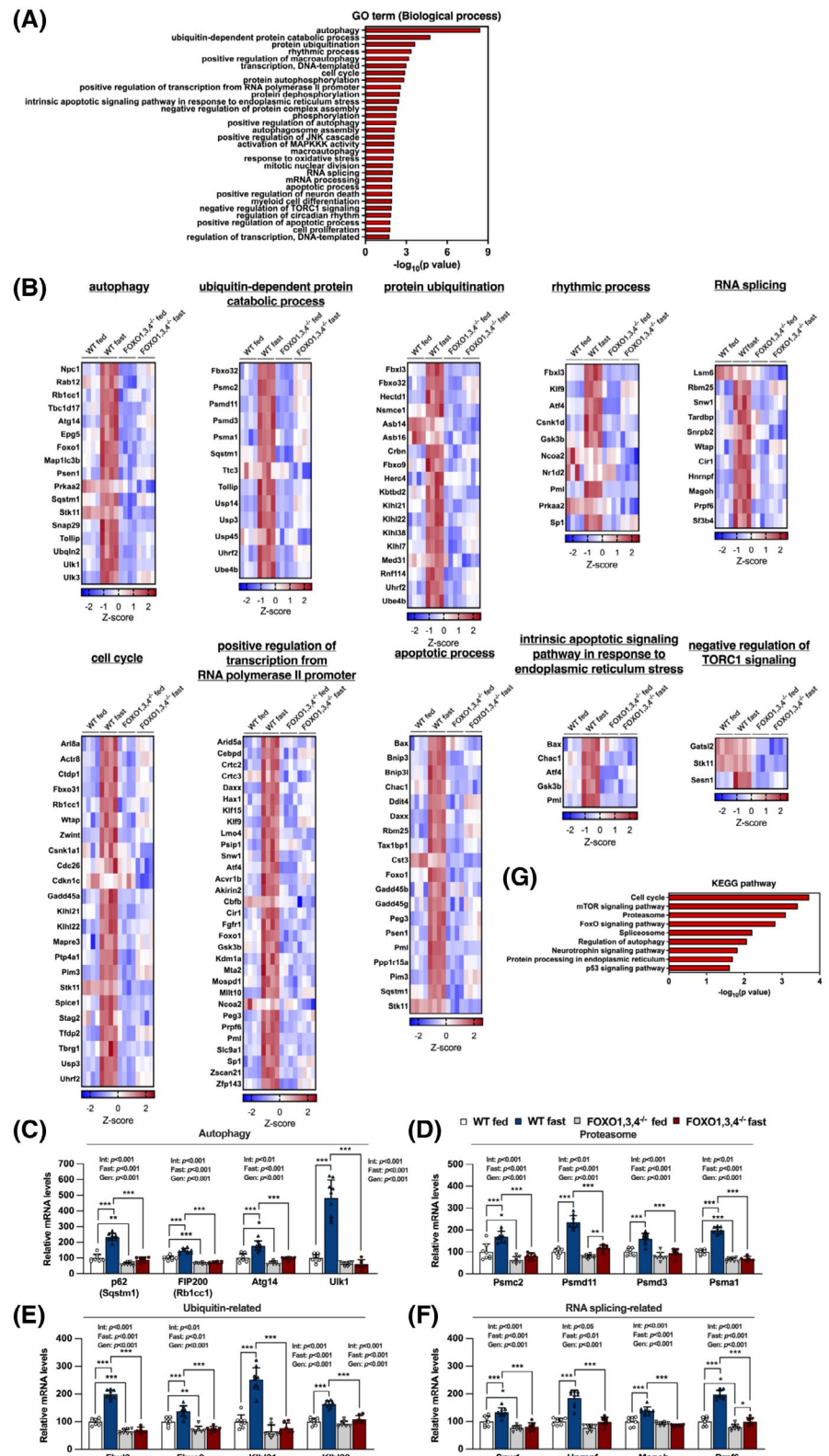


**FIGURE 2** FOXOs increase the abundance of C/EBP $\delta$ , activate the UPS, and conversely decrease p-4EBP1/4EBP1 levels in skeletal muscle during fasting. (A) Immunoblots and (B) densitometric analysis of C/EBP $\delta$ , ubiquitin, p-4EBP1 (Thr37/46), 4EBP1, p-S6K (Thr389), and S6K protein levels in the gastrocnemius of fed and 24 h-fasted and FOXO1,3a,4 $^{-/-}$  and WT mice ( $n = 5$  per group). (C) Immunoblots and densitometric analysis of p-4EBP1 (Thr37/46) and 4EBP1 protein levels in the quadriceps of FOXO1-Tg and control mice ( $n = 5$  per group). (D, E) Quantitative RT-PCR of the authentic FOXO1 (or FOXO3a) target muscle atrophy-related genes in (D) the quadriceps from fed and 24 h-fasted FOXO1,3a,4 $^{-/-}$  and WT mice ( $n = 7-9$  mice per group) and (E) the gastrocnemius from the FOXO1-Tg and control mice ( $n = 5-6$  per group). All data were normalized to 36B4 expression and represented as relative to control mice expression values. Values are mean  $\pm$  SD. \* $p < .05$ , \*\* $p < .01$ , and \*\*\* $p < .001$ . †† $p < .01$ , and ††† $p < .001$ ; genotype main effect (two-way ANOVA). (B, D) Fasting effects (Fast), genotype effects (Gen), and interaction between fasting and genotype effects (Int) were analyzed by two-way ANOVA followed by Tukey's post hoc test and (C, E) Student's two-tailed unpaired  $t$ -test

**FIGURE 3** FOXOs regulate the genes involved in the UPS, autophagy, cell cycle, spliceosome, apoptotic signaling, and mTOR signaling during fasting. (A) Gene ontology (GO) enrichment analysis in biological process in differentially expressed genes (DEGs) downregulated in 24 h-fasted FOXO1,3a,4<sup>-/-</sup> mice compared to 24 h-fasted WT mice with false discovery rate (FDR) of <0.05. (B) Heatmap showing the representative gene lists categorized by GO terms downregulated in 24 h-fasted FOXO1,3a,4<sup>-/-</sup> muscle versus 24 h-fasted WT muscle. Red and blue colors represent high and low expression levels, respectively. (C–F) Quantitative RT-PCR of the (C) autophagy genes, (D) proteasome genes, (E) ubiquitin-related genes, and (F) RNA splicing-related genes in the quadriceps from fed and 24 h-fasted FOXO1,3a,4<sup>-/-</sup> and WT mice ( $n = 7–9$  mice per group). (G) The KEGG pathway analysis in DEGs downregulated in 24 h-fasted FOXO1,3a,4<sup>-/-</sup> mice compared to 24 h-fasted WT mice with FDR of <0.05. All data were normalized to 36B4 expression and represented as relative to control mice expression values. Values are mean  $\pm$  SD. \* $p < .05$ , \*\* $p < .01$  and \*\*\* $p < .001$ . (C–F) Fasting effects (Fast), genotype effects (Gen), and interaction between fasting and genotype effects (Int) were analyzed by two-way ANOVA followed by Tukey's *post hoc* test



phosphorylation of S6K (another mTORC1 substrate), was not significantly increased in FOXO1,3a,4<sup>-/-</sup> mice (Figure S6A), implying that mTORC1/4EBP1 activation is substrate-specific (Figure 2A). In addition, phosphorylation of mTOR was not increased in FOXO1,3a,4<sup>-/-</sup> mice (Figure S6B). In FOXO1-Tg mice, however, the significant reduction of 4EBP1 Thr37/46

phosphorylation relative to total 4EBP1 was due to increased 4EBP1 protein expression, suggesting FOXO1 itself does not affect mTORC1 activity (Figure 2C). The above data support the concept that FOXOs activate the C/EBP $\delta$ -UPS-mediated proteolysis as well as to attenuate translation via the reduction of p-4EBP1/4EBP1 levels.

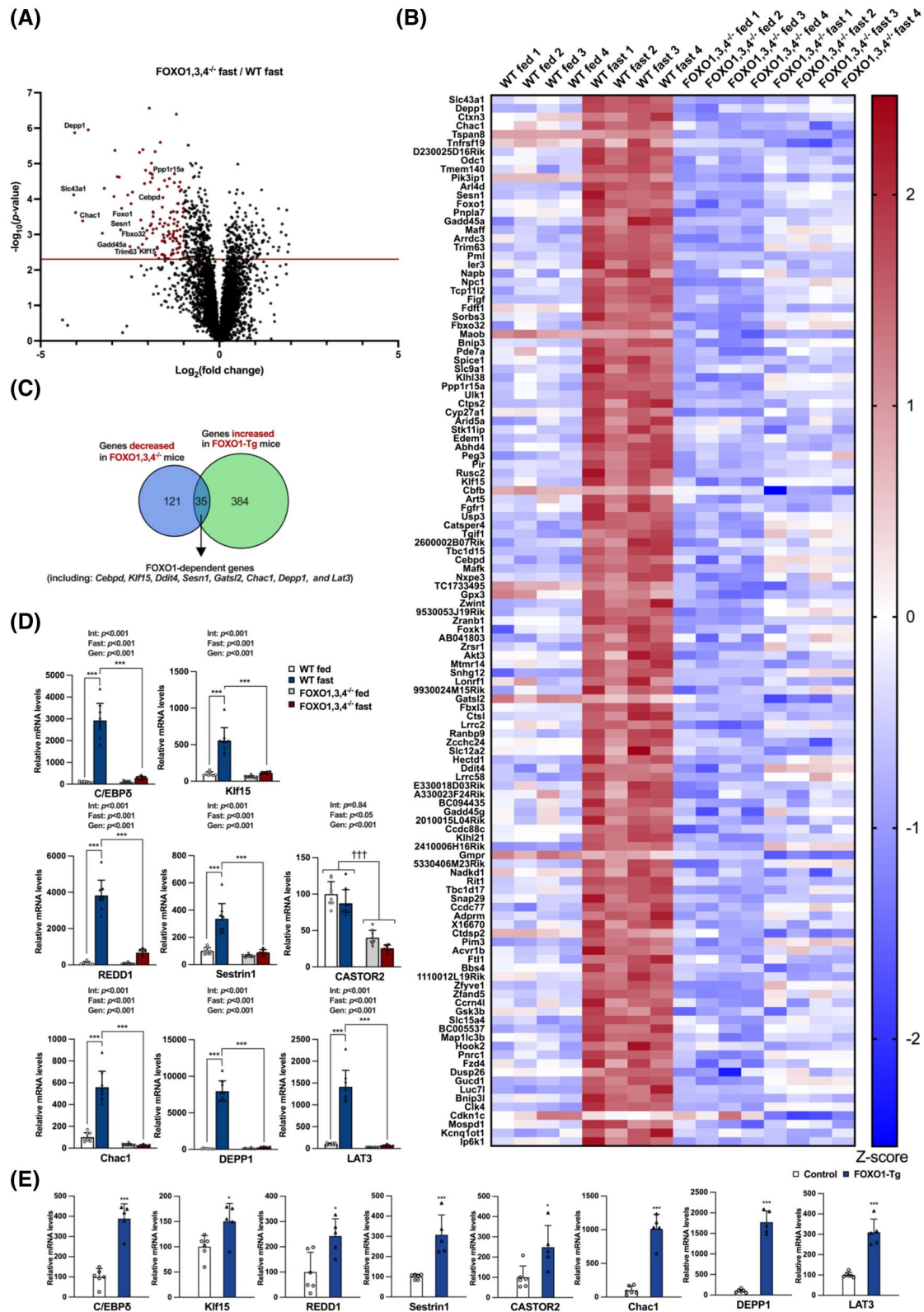


FIGURE 4 Legend on next page

### 3.4 | FOXO1 regulates atrophy-related genes in skeletal muscle in vivo

Muscle atrophy is reported to be caused by transcript regulation of certain atrophy-related genes.<sup>42,43</sup> We thus

investigated whether FOXOs induce expression of atrophy-related genes during fasting and if FOXO1 overexpression is sufficient to induce atrophy-related genes. Similar to up-regulated *Atrogin1* transcript expression, muscle-specific E3 ligase *MuRF1* transcript was significantly increased

in fasted WT muscle, but not in fasted FOXO1,3a,4<sup>-/-</sup> muscle (Figure 2D). Autophagy-related gene (*Cathepsin L*, *LC3b*, *Gabarapl1*) and other atrophy-related genes (*Gadd45α*, *4EBP1*, *Glul*, and *PDK4*) transcripts were also significantly increased in fasted WT muscle but not in fasted FOXO1,3a,4<sup>-/-</sup> muscle (Figure 2D). Additionally, analysis of transcript expression in FOXO1-Tg mice revealed up-regulated expression of atrophy-related gene (*Cathepsin L*, *Gabarapl1*, *Gadd45α*, *Atrogin1*, *4EBP1*, *Glul*, and *PDK4*) transcripts (Figure 2E), suggesting that some atrophy-related genes are intrinsically upregulated by FOXO1. Other autophagy-related genes such as *ATG5* and *Beclin1* were not up-regulated in fasted WT mice and FOXO1-Tg mice (Figure S7A,B). In FOXO1,3a,4<sup>-/-</sup> mice, *ATG5* and *Beclin1* expression were significantly downregulated (Figure S7A). These data demonstrate that FOXOs are involved in atrophy-related gene induction during fasting, and FOXO1 overexpression is sufficient for some of these responses.

### 3.5 | FOXOs regulate the genes involved in autophagy, the UPS, cell cycle, spliceosome, apoptotic signaling, and mTOR signaling during fasting

FOXOs function as transcription factors that directly regulate target gene expression; as such, we investigated the specific roles of FOXOs in transcriptional regulation during muscle atrophy. To achieve this, we performed microarray analysis on fed and fasted WT and FOXO1,3a,4<sup>-/-</sup> muscle. We observed a decrease in expression of 381 transcripts of the differentially expressed genes (DEGs) in fasted FOXO1,3a,4<sup>-/-</sup> mice with a false discovery rate (FDR) of <0.05 compared to fasted WT mice (Table S1). Gene ontology (GO) enrichment analysis was performed to elucidate the biological function of DEGs upregulated by FOXOs during fasting. The outcome of the analysis revealed enrichment in genes associated with biological

processes involving: “autophagy,” “ubiquitin-dependent protein catabolic process,” “rhythmic process,” “RNA splicing,” “cell cycle,” “positive regulation of transcription from RNA polymerase II promoter,” “intrinsic apoptotic signaling pathway in response to endoplasmic reticulum stress,” and “negative regulation of TORC1 signaling” (Figure 3A,B). Heatmap analysis demonstrated that these transcripts were under the control of FOXOs during fasting and some of these genes were validated by qRT-PCR (Figure 3B–F).

To further explore functional pathways regulated by FOXOs during fasting, we performed a KEGG pathway analysis. Top ranking significant pathways detected included previously established FOXO-regulated pathways<sup>44</sup> involved in “cell cycle,” “proteasome,” “FOXO signaling pathway,” and “autophagy,” confirming the validity of microarray data for the detection of functional pathways under the control of FOXOs (Figure 3G). Importantly, previously unrecognized pathways were also detected: “mTOR signaling pathway,” “spliceosome,” and “protein processing in the endoplasmic reticulum (ER)”. Together, the GO terms and KEGG pathway enrichment results indicated that FOXOs are required for the regulation of genes involved in UPS, autophagy, cell cycle, spliceosome, mTOR signaling, and ER stress-induced intrinsic apoptotic signaling during fasting.

### 3.6 | Identification of novel FOXO1 target genes including C/EBPδ using the gain- and loss-of-function model mice of FOXOs

Given the critical roles of FOXOs for muscle atrophy and the data that FOXO1 overexpression was sufficient to induce some atrophy-related genes (Figure 2E), we tried to identify novel FOXO1 target genes in vivo. To achieve this, we first sought to establish the identity of genes strongly induced by FOXOs

**FIGURE 4** Novel FOXO1 target genes identification in skeletal muscle during fasting. (A) Volcano plots showing the distribution of the differentially expressed genes in 24 h-fasted FOXO1,3a,4<sup>-/-</sup> mice versus 24 h-fasted WT mice on the log<sub>2</sub> scale. Red parallel lines highlight -log<sub>10</sub> p-value of .005 [false discovery rate (FDR) <0.05]. Red plots show the 121 genes that meet the criteria of [FDR of <0.05 and log<sub>2</sub>(fold change) of <-1]. (B) Heatmap showing the 121 genes downregulated in 24 h-fasted FOXO1,3a,4<sup>-/-</sup> muscle versus 24 h-fasted WT muscle showed as red plots on the volcano plots (Red and blue colors represent high and low expression levels, respectively). (C) The Venn diagram shows the overlap between 121 genes downregulated in 24 h-fasted FOXO1,3a,4<sup>-/-</sup> muscle versus 24 h-fasted WT muscle (blue circle) and the 384 genes upregulated in FOXO1-Tg mice (more than 1.5-fold compared to control mice) (green circle). The overlapping part shows 35 genes that were oppositely regulated in both the FOXO1,3a,4<sup>-/-</sup> mice and the FOXO1-Tg mice. (D and E) Quantitative RT-PCR of the novel FOXO1 target genes in (D) the quadriceps from fed and 24 h-fasted FOXO1,3a,4<sup>-/-</sup> and WT mice (*n* = 7–9 per group) and (E) the gastrocnemius from the FOXO1-Tg and control mice (*n* = 5–6 per group). All data were normalized to 36B4 expression and are shown as relative values to the control mice. Values are mean ± SD. \**p* < .05 and \*\*\**p* < .001. †††*p* < .001; genotype main effect (two-way ANOVA). (D) Fasting effects (Fast), genotype effects (Gen), and interaction between fasting and genotype effects (Int) were analyzed by two-way ANOVA followed by Tukey's *post hoc* test and (E) Student's two-tailed unpaired *t*-test

**TABLE 1** List of 35 genes whose expression levels were upregulated in FOXO1-Tg mice compared to WT control mice and downregulated in skeletal muscle of fasted FOXO1,3,4<sup>-/-</sup> mice compared to fasted WT mice

Systematic Name	Gene Name	WT fed average	WT fast average	FOXO1,3,4 <sup>-/-</sup> fed average	FOXO1,3,4 <sup>-/-</sup> fast average	Log <sub>2</sub> fold change (FOXO1,3,4 <sup>-/-</sup> fast/WT fast)	-log <sub>10</sub> p value (FOXO1,3,4 <sup>-/-</sup> fast/WT fast)	Fold change (FOXO1-Tg/WT)	Description
1	NM_001081349	5.47951	9.19400	4.12258	5.06161	-4.0727	4.1168	2.5044	Solute carrier family 43, member 1 (Slc43a1), transcript variant 1
2	NM_145980	5.54159	10.85669	5.15955	6.80549	-4.0443	5.8692	28.1238	RIKEN cDNA 8430408G22 gene (8430408G22Rik), transcript variant 1
3	NM_001134697	5.73815	8.02748	3.44694	4.09039	-4.0222	3.6209	10.5972	Cortexin 3 (Ctxn3)
4	NM_026929	8.81521	11.08778	7.63474	7.18034	-3.8238	3.3831	3.3656	ChaC, cation transport regulator 1 (Chacl)
5	NM_013869	6.19129	7.06946	5.03569	3.88984	-3.2733	3.0335	3.2289	Tumor necrosis factor receptor superfamily, member 19 (Tnfrsf19)
6	NM_145604	5.73937	8.64564	5.19436	5.44856	-3.2188	4.3017	2.5404	RIKEN cDNA D230025D16 gene (D230025D16Rik)
7	NM_013614	4.91629	7.55233	4.19084	4.61035	-2.9485	4.0731	3.3050	Ornithine decarboxylase, structural 1 (Odc1)
8	NM_197986	8.05399	11.25681	7.36595	8.32690	-2.9212	5.3717	2.5806	Transmembrane protein 140 (Tmem140)
9	NM_025404	4.49251	8.03059	4.32218	5.24619	-2.7990	4.6189	4.9226	ADP-ribosylation factor-like 4D (Arl4d)
10	NM_001162908	6.23455	9.26988	5.72811	6.58500	-2.7612	3.1314	2.2103	Sestrin 1 (Sesn1), transcript variant 1
11	NM_019739	6.05201	8.34216	4.61407	5.64361	-2.7344	3.7394	56.5392	Forkhead box O1 (Foxo1)
12	NM_146251	6.10547	8.04014	4.98293	5.50018	-2.5596	4.1132	2.5811	Patatin-like phospholipase domain containing 7 (Pnpla7)
13	NM_007836	5.20524	7.98777	5.17555	5.57291	-2.5002	2.6614	7.6088	Growth arrest and DNA-damage-inducible 45 alpha (Gadd45a)
14	NM_178087	5.70806	7.75567	5.62118	5.52622	-2.2353	5.3159	2.6839	Promyelocytic leukemia (Pml), transcript variant 2
15	NM_172778	6.61956	6.50151	4.39941	4.54127	-1.9601	6.5643	1.9582	Monoamine oxidase B (Maob), nuclear gene encoding mitochondrial protein
16	NM_016981	6.61769	8.23746	6.61119	6.36134	-1.9029	3.2981	1.5701	Solute carrier family 9 (sodium/hydrogen exchanger), member 1 (Slc9a1)
17	NM_001290726	4.91104	6.88865	5.28468	5.01497	-1.8537	3.1464	2.1218	AT rich interactive domain 5A (MRF1-like) (Arid5a), transcript variant 1
18	NM_023184	6.03361	8.05331	5.46546	6.36088	-1.7319	2.6058	1.6125	Kruppel-like factor 15 (Klf15)
19	NM_001161458	10.17687	10.18622	9.37078	8.43064	-1.6949	2.3251	1.5233	Core binding factor beta (Cbfb), transcript variant 4
20	NM_010206	4.63860	5.94950	4.37294	4.29888	-1.6704	3.3067	1.7881	Fibroblast growth factor receptor 1 (Fgfr1), transcript variant 1

TABLE 1 (Continues)

Systematic Name	Gene Name	WT fed average	WT fast average	FOXO1,3,4 <sup>-/-</sup> fed average	FOXO1,3,4 <sup>-/-</sup> fast average	Log <sub>2</sub> fold change (FOXO1,3,4 <sup>-/-</sup> fast/WT fast)	-log <sub>10</sub> p value (FOXO1,3,4 <sup>-/-</sup> fast/WT fast)	Fold change (FOXO1-Tg/WT)	Description
21	NM_007679	8.32526	11.50969	8.17850	9.93831	-1.5801	4.0419	2.8819	CCAAT/enhancer binding protein (C/EBP), delta (Cebpd)
22	NM_008161	7.91434	8.37977	6.45446	6.85548	-1.5487	2.9073	3.6635	Glutathione peroxidase 3 (Gpx3)
23	NM_207302	6.96369	8.21294	6.35262	6.69562	-1.5273	3.3180	1.6137	Zinc finger, RAN-binding domain containing 1 (Zranb1)
24	NR_110469	5.23827	7.74066	5.17519	6.20718	-1.5236	2.4028	1.7890	Brain cDNA, clone MNCB-1768.
25	ENSMUST0000016088	5.79143	5.52617	4.71155	4.08677	-1.4194	3.0820	1.5949	Ens/GATS protein-like 2 [Source:MGI Symbol;Acc:MGI:1933384]
26	NM_009984	9.43806	10.64310	9.27248	9.26810	-1.3922	3.0162	2.6302	Cathepsin L (Ctsl)
27	NM_001101433	9.10181	9.90342	8.79354	8.53726	-1.3595	3.6226	2.4787	Zinc finger, CCHC domain containing 24 (Zcchc24)
28	NM_009194	7.85672	8.65304	7.56522	7.34263	-1.3459	2.4177	1.6013	Solute carrier family 12, member 2 (Slc12a2)
29	NM_029083	8.05168	11.78433	7.44343	10.47231	-1.3040	2.9435	2.5019	DNA-damage-inducible transcript 4 (Ddit4), mRNA [NM_029083]
30	AK017236	7.19480	9.04385	6.70590	7.80756	-1.2497	2.8949	1.8920	Adult male pituitary gland cDNA, RIKEN full-length enriched library, clone:530406M23 product:unclassifiable, full insert sequence.
31	NM_023348	5.26298	6.29150	5.02815	5.11460	-1.1903	2.8160	1.7127	Synaptosomal-associated protein 29 (Snap29)
32	NM_133895	7.95723	9.33700	7.97050	8.23397	-1.1001	4.4775	1.5058	Solute carrier family 15, member 4 (Slc15a4)
33	NM_008055	7.27649	8.20797	6.77396	7.20099	-1.0290	2.3204	2.5953	Frizzled homolog 4 (Drosophila) (Fzd4)
34	NM_025869	8.10190	8.94659	7.33909	7.89961	-1.0264	2.4882	3.4978	Dual specificity phosphatase 26 (putative) (Dusp26)
35	NM_009876	7.77690	7.41299	7.71396	6.40440	-1.0044	3.7366	4.1499	Cyclin-dependent kinase inhibitor 1C (P57) (Cdkn1c), transcript variant 2

Note: Gene expression signal were converted to the log<sub>2</sub> scale. Listed 35 genes among 381 genes listed in Supporting Information Table S1 were upregulated in FOXO1-Tg mice (more than 1.5-fold compared to control mice). "Gene name" means the gene symbol of each gene.

with more stringent criteria. Volcano plots detected 121 significantly downregulated DEGs [FDR of  $<0.05$ ,  $\log_2(\text{fold change})$  of  $<-1$ ] in FOXO1,3a,4<sup>-/-</sup> muscle during fasting, which were visualized by heatmap (Figure 4A,B). We considered that among the strongly downregulated 121 DEGs in FOXO1,3a,4<sup>-/-</sup> muscle, the genes induced by FOXO1 overexpression would be novel FOXO1 target genes in skeletal muscle. Thus, we compared FOXO1,3a,4<sup>-/-</sup> and FOXO1-Tg mice transcriptome and obtained 35 potential novel FOXO1 target genes, including transcription factors involved in muscle atrophy [*Cebpd* (C/EBP $\delta$ ) and *Klf15* (KLF15)],<sup>16,17,45-47</sup> mTORC1 negative regulators [*Ddit4* (Redd1), *Sesn1* (Sestrin1) and *Gatsl2* (Castor2)],<sup>48-51</sup> unfolded protein response [*Chac1* (Chac1)],<sup>52</sup> autophagy regulator [*Depp1* (Depp1)],<sup>53</sup> and amino acid transporter [*Slc43a1* (Lat3)]<sup>54</sup> (Figure 4C, Table 1). The qRT-PCR analysis confirmed the microarray data. *C/EBP $\delta$*  and *Klf15* transcripts significantly increased in fasted WT muscle, but not in fasted FOXO1,3a,4<sup>-/-</sup> muscle (Figure 4D), suggesting that FOXOs promote muscle atrophy via the induction of these atrophy-related transcription factors.

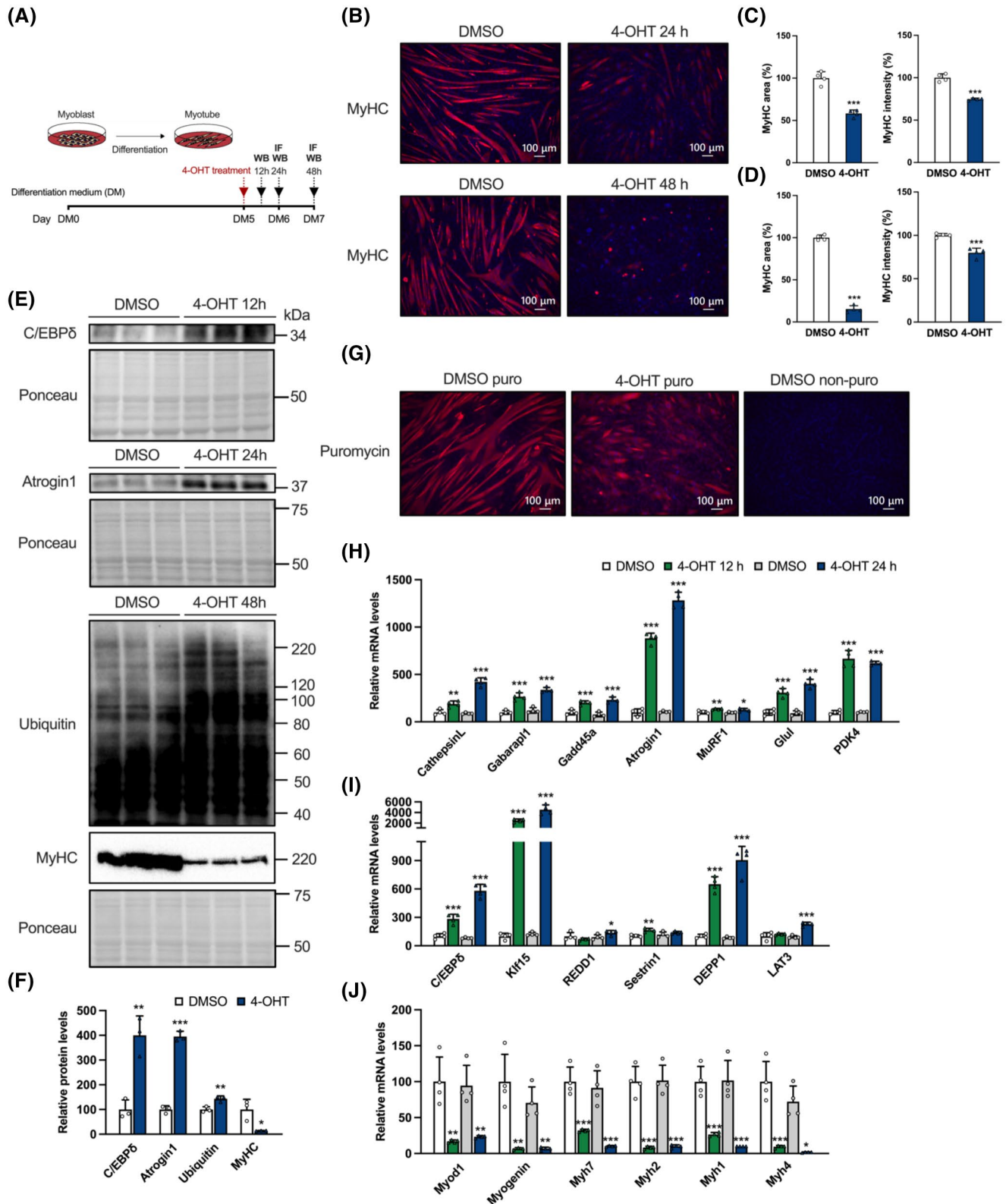
mTORC1 is a crucial protein synthesis regulator whose activity is regulated by multiple upstream negative regulators, including Redd1, Sestrin1 (a most abundant isoform of Sestrins in skeletal muscle),<sup>55</sup> and Castor2 (most abundant isoform of Castors in skeletal muscle).<sup>51</sup> Parallel to the observation that FOXOs could be required for the regulation of mTORC1 signaling via the inhibition of mTORC1/4EBP1 axis in skeletal muscle (Figure 2A-C), *Redd1* and *Sestrin1* transcripts significantly increased in fasted WT muscle but not in fasted FOXO1,3a,4<sup>-/-</sup> muscle (Figure 4D). The previous report demonstrated that FOXOs inhibit mTORC1 by inducing *Sestrin3* expression.<sup>56</sup> Given Sestrin1 is the most abundant isoform of Sestrins in skeletal muscle, FOXOs may inhibit mTORC1 by inducing *Sestrin1* expression in skeletal muscle during fasting. *Castor2* transcript did not increase during fasting but markedly decreased in

FOXO1,3a,4<sup>-/-</sup> mice under both fed and fasting conditions (Figure 4D), indicating that FOXOs are required for maintaining the basal *Castor2* transcript level.

Other genes that increased in a FOXOs-dependent manner during fasting include *Chac1*, *Depp1*, and *Lat3*, all of which are lowly expressed in skeletal muscle stimulated with insulin in vivo (decreased FOXO signaling<sup>57</sup>).<sup>58</sup> LAT3 is an amino acid transporter that transports leucine, isoleucine, valine (BCAA), and phenylalanine into cells.<sup>54</sup> We thus measured skeletal muscle amino acid levels in WT (fed and fasted) and FOXO1,3a,4<sup>-/-</sup> mice (fed and fasted). Consistent with the induction of *Lat3* transcript in fasted WT muscle, leucine, and isoleucine levels were significantly increased in fasted WT muscle, but these responses were completely abolished in fasted FOXO1,3a,4<sup>-/-</sup> muscle (Figure S8), suggesting that FOXO-dependent *Lat3* transcript functionally leads to increased BCAA levels in skeletal muscle during fasting. Given the skeletal muscle is the central tissue of BCAA catabolism, which is activated during glucocorticoid-induced muscle atrophy at least in part via the *Klf15*-branched-chain aminotransferase 2 (BCAT2) axis,<sup>45</sup> FOXO1-induced LAT3 could contribute to the increased abundance of intramuscular BCAA to supply energy source during fasting. Importantly, *C/EBP $\delta$* , *Klf15*, *Redd1*, *Sestrin1*, *Castor2*, *Chac1*, *Depp1*, and *Lat3* transcripts significantly increased in FOXO1-Tg mice versus control mice, indicating that FOXO1 overexpression was sufficient for the induction of these genes (Figure 4E).

Taken together, the above data strongly suggest that FOXOs are crucial factors in the induction of atrophy-related genes in skeletal muscle and that FOXO1 overexpression is sufficient for these responses in vivo. Thus, including the latter experiment, we identified *C/EBP $\delta$* , *Redd1*, *Sestrin1*, *Castor2*, *Chac1*, *Depp1*, and *Lat3* as novel FOXO1 target genes in the skeletal muscle.

**FIGURE 5** FOXO1 activates the expression of C/EBP $\delta$ , the UPS, and decreases MyHC in C2C12 myotubes. (A) C2C12 myoblasts expressing FOXO1-ER fusion proteins (FOXO1-ER) were differentiated into myotubes for 5 days and treated with 4-OHT or DMSO to induce FOXO1 nuclear translocation to determine effects on myotube atrophy and activation of UPS-mediated proteolysis. (B-D) (B) C2C12 myotubes expressing FOXO1-ER treated with 4-OHT or DMSO for 24 h (top) and 48 h (bottom) were stained and visualized using immunofluorescence (IF) with an anti-myosin heavy chain (MyHC) antibody. Representative images are shown from two independent experiments. Scale bar = 100  $\mu\text{m}$ . Nuclei were stained with DAPI (blue). Quantification of MyHC positive area (left) and MyHC intensity (right) in C2C12 myotubes expressing FOXO1-ER treated with 4-OHT or DMSO for 24 h (C) and 48 h (D) ( $n = 4$  sets of cells per group). (E, F) (E) Western blotting (WB) and (F) densitometric analysis of C/EBP $\delta$  (at 12 h), Atrogin1 (at 24 h), ubiquitin (at 48 h), MyHC (at 48 h) protein levels in C2C12 myotubes expressing FOXO1-ER treated with 4-OHT or DMSO for 12, 24, and 48 h ( $n = 3$  sets of cells per group). (G) C2C12 myotubes expressing FOXO1-ER were treated with 4-OHT or DMSO for 48 h and subsequently left untreated (non-puro) or labeled with 1  $\mu\text{M}$  puromycin (puro) for 30 min, which were stained and visualized using immunofluorescence (IF) with an anti-puromycin antibody (SUnSET method). Representative images are shown. Scale bar = 100  $\mu\text{m}$ . Nuclei were stained with DAPI (blue). (H-J) Quantitative RT-PCR of (H) authentic FOXO1 (or FOXO3a) target genes, (I) novel FOXO1 target genes, and (J) myogenic regulatory factor and myosin heavy chain genes in C2C12 myotubes expressing FOXO1-ER treated with 4-OHT or DMSO for 12 and 24 h ( $n = 4$  sets of cells per group). All data were normalized with 36B4 expression and are shown as relative values to the control group (open bars). Values are mean  $\pm$  SD. \* $p < .05$ , \*\* $p < .01$ , and \*\*\* $p < .001$ . (Student's two-tailed unpaired  $t$ -test or Mann-Whitney  $U$ -test)



### 3.7 | Activation of FOXO1 in C2C12 myoblasts promotes novel FOXO1 target gene expression

To examine whether the novel FOXO1 target genes described above are regulated by FOXO1 in a cell-autonomous

manner, we investigated changes in target gene expression in C2C12 myoblasts, expressing constitutively-active FOXO1, and estrogen receptor fusion protein (FOXO1-ER), treated and activated with 4-hydroxytamoxifen (4-OHT) in vitro. Treatment with 4-OHT induces FOXO1-ER nuclear translocation and subsequent FOXO1-mediated

transcription of target genes.<sup>39</sup> Expression of previously established FOXO target genes (*Cathepsin L*, *Gabarapl1*, *Gadd45a*, *Atrogin1*, *MuRF1*, *Glul*, and *PDK4*) (Figure S9A) increased. Interestingly, expression of novel FOXO1 target genes (*C/EBPδ*, *Klf15*, *Redd1*, *Castor2*, *Chac1*, *Depp1*, and *Lat3*) identified in vivo, significantly increased in response to 4-OHT in C2C12 myoblasts (Figure S9B,C); indicating that these transcripts are induced in the skeletal muscle in a cell-autonomous manner. Taken together, these findings strongly suggest that the above-mentioned novel genes are potential targets of FOXO1 since their expression is significantly induced by FOXO1 both in vivo and in vitro.

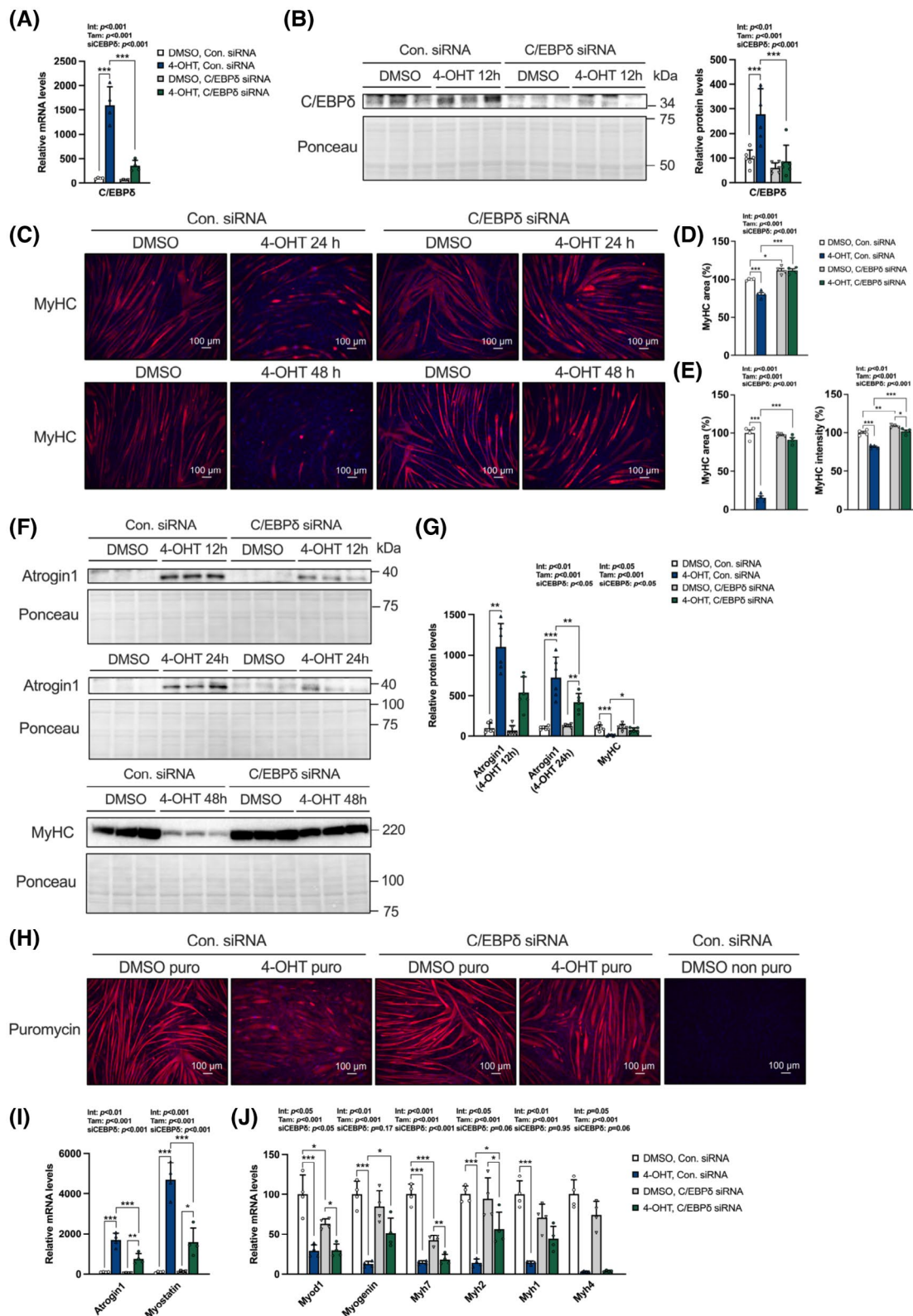
### 3.8 | FOXO1 activates C/EBPδ expression, UPS, and decreases MyHC in C2C12 myotubes

Given our in vivo finding that C/EBPδ abundance increased in a FOXO-dependent manner during fasting, we hypothesized that the FOXO1–C/EBPδ signaling pathway is responsible for the FOXO1-mediated UPS and muscle loss. Studies have reported that C/EBPδ KO mice are resistant to muscle atrophy in chronic kidney disease and cancer cachexia<sup>16,17</sup> and C/EBPδ increases the promoter activity of E3 ubiquitin ligases, Atrogin1 and MuRF1.<sup>16</sup> A strong induction of C/EBPδ was also observed by dexamethasone administration or starvation.<sup>59,60</sup> Furthermore, activated STAT3 (p-STAT3) has also been shown to increase C/EBPδ

expression.<sup>17</sup> However, the association between FOXO1 and C/EBPδ has not been reported by previous studies. Therefore, we investigated whether activation of FOXO1 is sufficient to increase C/EBPδ abundance and decrease MyHC abundance in myotubes (Figure 5A).

Although the myotube diameter was not affected (Figure S10A), FOXO1 activation in C2C12 myotubes induced robust myofiber loss as measured by the MyHC positive area and MyHC intensity (Figure 5B–D) with increased abundance of C/EBPδ and E3 ligase Atrogin1, increasing total ubiquitinated protein levels and loss of MyHC protein (Figure 5E,F). To investigate whether the decrease of MyHC protein in FOXO1 activation is due to increased degradation, we performed immunoprecipitation (IP) with antibody against MyHC and western blots with antibody against ubiquitin. FOXO1 activation did not increase MyHC polyubiquitination with or without MG-132, a proteasome inhibitor (Figure S10B). However, the treatment of the cells with MG132 partially prevented the loss of MyHC in FOXO1 activation, suggesting that FOXO1 indirectly decreased MyHC protein via the UPS (Figure S10B). To determine whether activated FOXO1 has a role in protein synthesis, we evaluated mTORC1 activity and protein synthesis by measuring phosphorylation of mTORC1 substrate (p-S6K/S6K and p-4EBP1/4EBP1) and puromycin incorporation into proteins of myotubes (SUnSET method),<sup>40</sup> respectively. The activation of FOXO1 in C2C12 myotubes attenuated phosphorylation of S6K and puromycin incorporation (Figures S10C and 5G), indicating that FOXO1

**FIGURE 6** FOXO1–C/EBPδ signaling is responsible for the induction of Atrogin1, Myostatin, and decrease of MyHC in C2C12 myotubes. (A and B) C2C12 myoblasts expressing FOXO1–ER fusion proteins (FOXO1–ER) were differentiated into myotubes for 5 days and transfected with either control siRNA (open and blue bars) or siRNA of C/EBPδ (gray and green bars). At 6 h after transfection, 4-OHT (1 μM, blue and green bars) or DMSO (control, open, and gray bars) were administrated into the culture medium. (A) At 24 h after 4-OHT treatment, quantitative RT-PCR of C/EBPδ was performed ( $n = 4$  sets of cells per group). (B) At 12 h after 4-OHT treatment, western blotting and densitometric analysis of C/EBPδ were performed ( $n = 6$  sets of cells per group from two independent experiments). (C) C2C12 myotubes expressing FOXO1–ER transfected with control siRNA or siRNA of C/EBPδ and after 6 h treated with 4-OHT or DMSO for 24 h (top) and 48 h (bottom) were stained and visualized using immunofluorescence with an anti-myosin heavy chain (MyHC) antibody. Representative images were shown from two independent experiments. Scale bar = 100 μm. Nuclei were stained with DAPI (blue). (D, E) Quantification of MyHC positive area and MyHC intensity in C2C12 myotubes expressing FOXO1–ER transfected with control siRNA (open and blue bars) or siRNA of C/EBPδ (gray and green bars) and after 6 h treated with 4-OHT or DMSO for 24 h (D) and 48 h (E) ( $n = 4$  sets of cells per group). (F, G) (F) Western blotting and (G) densitometric analysis of Atrogin1 (at 12 and 24 h), MyHC (at 48 h) protein levels in C2C12 myotubes expressing FOXO1–ER transfected with control siRNA (open and blue bars) or siRNA of C/EBPδ (gray and green bars) and after 6 h treated with 4-OHT or DMSO for 12, 24, and 48 h ( $n = 6$  sets of cells per group from two independent experiments). (H) C2C12 myotubes expressing FOXO1–ER transfected with control siRNA or siRNA of C/EBPδ and after 6 h treated with 4-OHT or DMSO for 48 h and subsequently left untreated (non-puro) or labeled with 1 μM puromycin (puro) for 30 min, which was stained and visualized using immunofluorescence with an anti-puromycin antibody (SUnSET method). Representative images were shown from two independent experiments. Scale bar = 100 μm. Nuclei were stained with DAPI (blue). (I, J) Quantitative RT-PCR of (I) Atrogin1 and Myostatin and (J) myogenic regulatory factor and myosin heavy chain genes in C2C12 myotubes expressing FOXO1–ER transfected with control siRNA or siRNA of C/EBPδ and after 6 h treated with 4-OHT or DMSO for 24 h ( $n = 4$  sets of cells per group). All data were normalized with GAPDH expression and are shown as relative values to the control group (open bars). Values are mean ± SD. \* $p < .05$ , \*\* $p < .01$ , and \*\*\* $p < .001$ . 4-OHT effects (Tam), siC/EBPδ effects (siC/EBPδ), and interaction between Tam and siC/EBPδ (Int) were analyzed by two-way ANOVA followed by Tukey's *post hoc* test



not only activates UPS-mediated proteolysis but could inhibit protein synthesis in C2C12 myotubes. However, phosphorylation of mTOR and its downstream target S6 ribosomal protein, as well as phosphorylation of 4EBP1, a second mTORC1 downstream target, did not decrease during FOXO1 activation in C2C12 myotubes

(Figure S10C). Phosphorylation of eIF2 $\alpha$ , a critical ribosome assembly initiation factor, reduced in FOXO1-activated C2C12 myotubes, possibly because FOXO1 activation for 24h resulted in the upregulation of *Gadd34* transcript, a downstream target of the integrated stress response (ISR) with phosphatase activity toward eIF2 $\alpha$ <sup>61</sup>

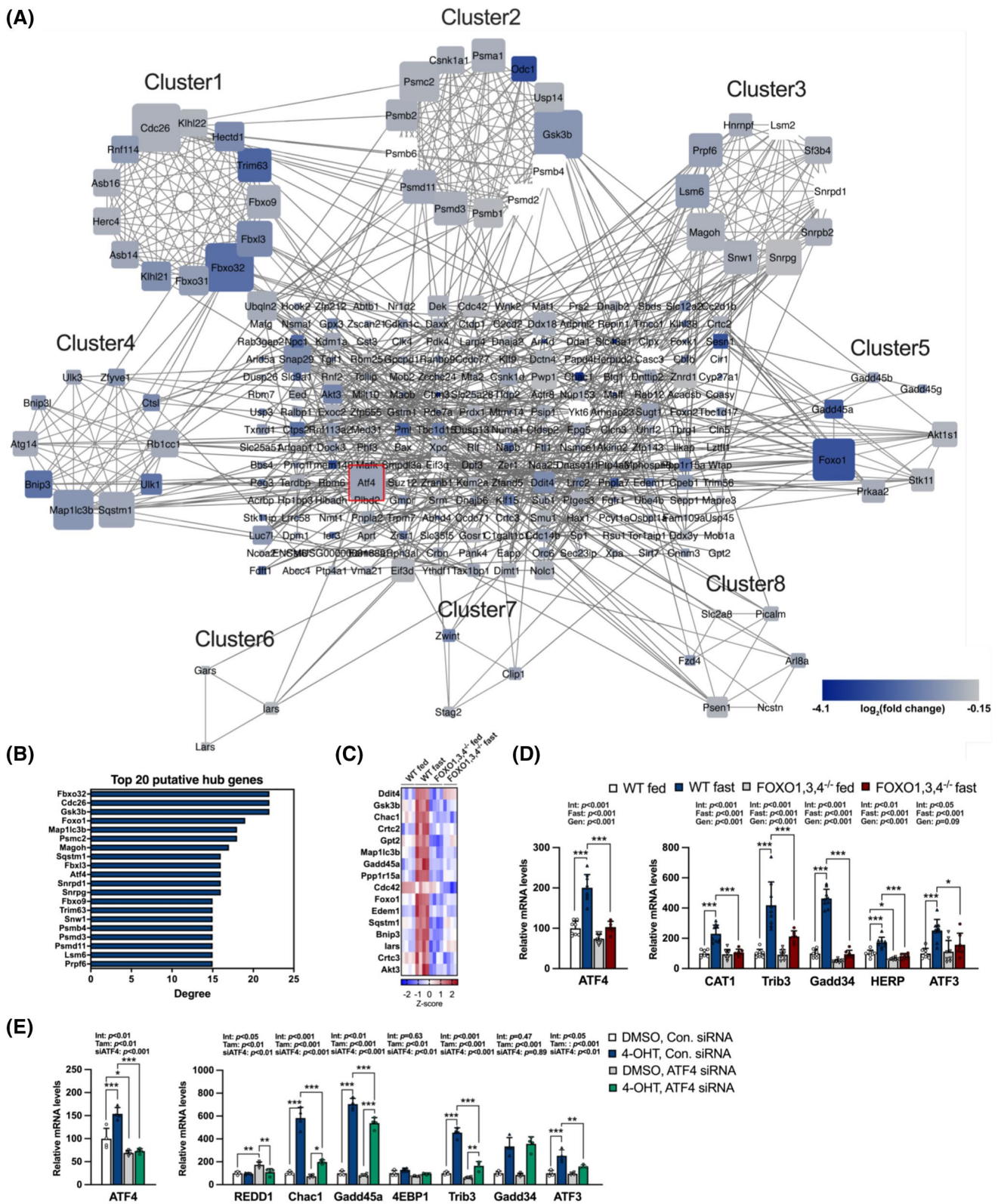


(Figure S10C,D). To further support the muscle atrophy phenotype, we examined gene expression changes of several muscle atrophy-related genes, novel FOXO1 target genes, and myogenic regulatory factor genes. Transcript expression of both established muscle atrophy-related

genes (*Cathepsin L*, *Gabarapl1*, *Gadd45a*, *Atrogin1*, *MuRF1*, *Glul*, and *PDK4*) and novel FOXO1 target genes (*C/EBP $\delta$* , *Klf15*, *Redd1*, *Sestrin1*, *Depp1*, and *Lat3*) robustly increased in FOXO1-activated myotubes (Figure 5H,I). Conversely, the expression of myogenic

regulatory factor (*Myod1* and *Myogenin*) and MyHC (*Myh7*, *Myh2*, *Myh1*, and *Myh4*) (Figure 5J) genes robustly decreased in FOXO1-activated C2C12 myotubes, suggesting the loss of myogenic property by FOXO1 in mature myotubes. Based on these findings, we deduce the following: FOXO1 activates C/EBP $\delta$  and the UPS, induces the loss of myogenic property, resulting in a robust decrease of MyHC in C2C12 myotubes.

### 3.9 | FOXO1-regulated C/EBP $\delta$ expression is responsible for the activation of Atrogin1, Myostatin, and decreased MyHC in C2C12 myotubes

To test the hypothesis that the FOXO1–C/EBP $\delta$  signaling pathway is responsible for the FOXO1-mediated UPS and muscle loss, we next investigated whether the FOXO1-induced activation of UPS and decreased MyHC requires C/EBP $\delta$  by performing a loss-of-function experiment for C/EBP $\delta$ . C/EBP $\delta$  was knocked down using siRNA in C2C12 myotubes expressing FOXO1-ER in which the increased expression of C/EBP $\delta$  transcript by 4-OHT treatment (FOXO1 activation) was suppressed to ~30% in C2C12 myotubes transfected with siC/EBP $\delta$  (Figure 6A, vs. control siRNA). Western blot analysis confirmed that C/EBP $\delta$  protein levels markedly increased in FOXO1-activated C2C12 myotubes, whereas the increase in C/EBP $\delta$  protein abundance was significantly attenuated in FOXO1-activated C2C12 myotubes transfected with siC/EBP $\delta$  (Figure 6B, vs. control siRNA). Immunofluorescent staining for MyHC in FOXO1-activated C2C12 myotubes showed that FOXO1-induced robust decrease in MyHC was abolished in FOXO1-activated C2C12 myotubes transfected with siC/EBP $\delta$  as measured by the MyHC

positive area and MyHC intensity (Figures 6C–E and S10A).

Notably, western blot analysis revealed that marked induction of E3 ligase Atrogin1 and loss of MyHC during FOXO1 activation was significantly attenuated in siC/EBP $\delta$ -treated C2C12 myotubes (Figure 6F,G), suggesting that FOXO1–C/EBP $\delta$  signaling is responsible for the FOXO1-mediated UPS and muscle loss. Furthermore, the decreased puromycin incorporation into proteins of myotubes by FOXO1 activation was also blunted in C2C12 myotubes transfected with siC/EBP $\delta$  (Figure 6H). These findings were further corroborated by the results that, in siC/EBP $\delta$ -treated C2C12 myotubes, FOXO1-induced *Atrogin1*, and *Myostatin* transcript and decreased expression of myogenic regulatory factor (*Myogenin*), and MyHC (*Myh2* and *Myh1*) genes were abolished (Figure 6I,J), indicating that induction of UPS and the suppression of myogenic differentiation by FOXO1, at least in part, requires the induction of C/EBP $\delta$ . Therefore, we identify C/EBP $\delta$  as the critical factor responsible for the activation of FOXO1-induced Atrogin1, Myostatin, and decreased MyHC in C2C12 myotubes.

### 3.10 | The protein–protein interaction network analysis identified ATF4 as a key transcription factor among FOXOs-regulated DEGs during fasting

To further search for the putative hub genes regulated by FOXOs during fasting, we constructed the protein–protein interaction networks from FOXO-regulated DEGs during fasting using the STRING database<sup>37</sup> (Figure 7A). This network analysis identified the putative hub genes with a large number of direct edges (protein–protein interaction) (Top 20 genes are shown in

**FIGURE 7** The protein-protein interaction network analysis identified ATF4 as a hub transcription factor among FOXOs-regulated DEGs during fasting. (A) The protein-protein interaction network of differentially expressed genes (DEGs) downregulated in 24 h-fasted FOXO1,3a,4<sup>-/-</sup> mice compared to 24 h-fasted WT mice with a false discovery rate (FDR) of <0.05. 284 nodes and 708 interactions were detected. The color of nodes indicates log<sub>2</sub> fold change values, and the circle size of nodes indicates the number of direct edges (degree). (B) The top 20 putative hub genes were identified by the protein-protein interaction network analysis. (C) Heatmap showing the predicted 16 genes with the direct edges to ATF4. Red and blue colors represent high and low expression levels, respectively. (D) Quantitative RT-PCR of ATF4 and ATF4 target genes (*Cat1*, *Trib3*, *Gadd34*, *Herp*, and *ATF3*) in the quadriceps from fed and 24 h-fasted FOXO1,3a,4<sup>-/-</sup> and WT mice ( $n = 7–9$  per group). All data were normalized to 36B4 expression and are shown as relative values to the control mice. Values are mean  $\pm$  SD. \* $p < .05$  and \*\*\* $p < .001$ . Fasting effects (Fast), genotype effects (Gen), and interaction between fasting and genotype effects (Int) by two-way ANOVA followed by Tukey's *post hoc* test. (E) C2C12 myoblasts expressing FOXO1-ER fusion protein were transfected with control siRNA (open and blue bars) or siRNA of ATF4 (gray and green bars). At 6 h after transfection, 4-OHT (1  $\mu$ M, blue and green bars) or DMSO (control, open and gray bars) were administrated into the culture medium. After 24 h, quantitative RT-PCR of ATF4 and ATF4 target genes (*Redd1*, *Chac1*, *Gadd45a*, *4EBP1*, *Trib3*, *Gadd34*, and *ATF3*) were performed in each cell ( $n = 4$  sets of cells per group). All data were normalized with 18S expression and are shown as relative values to the control group (open bars). Values are mean  $\pm$  SD. \* $p < .05$ , \*\* $p < .01$ , and \*\*\* $p < .001$ . 4-OHT effects (Tam) or siATF4 effects (siATF4), and interaction between Tam and siATF4 (Int) by two-way ANOVA followed by Tukey's *post hoc* test

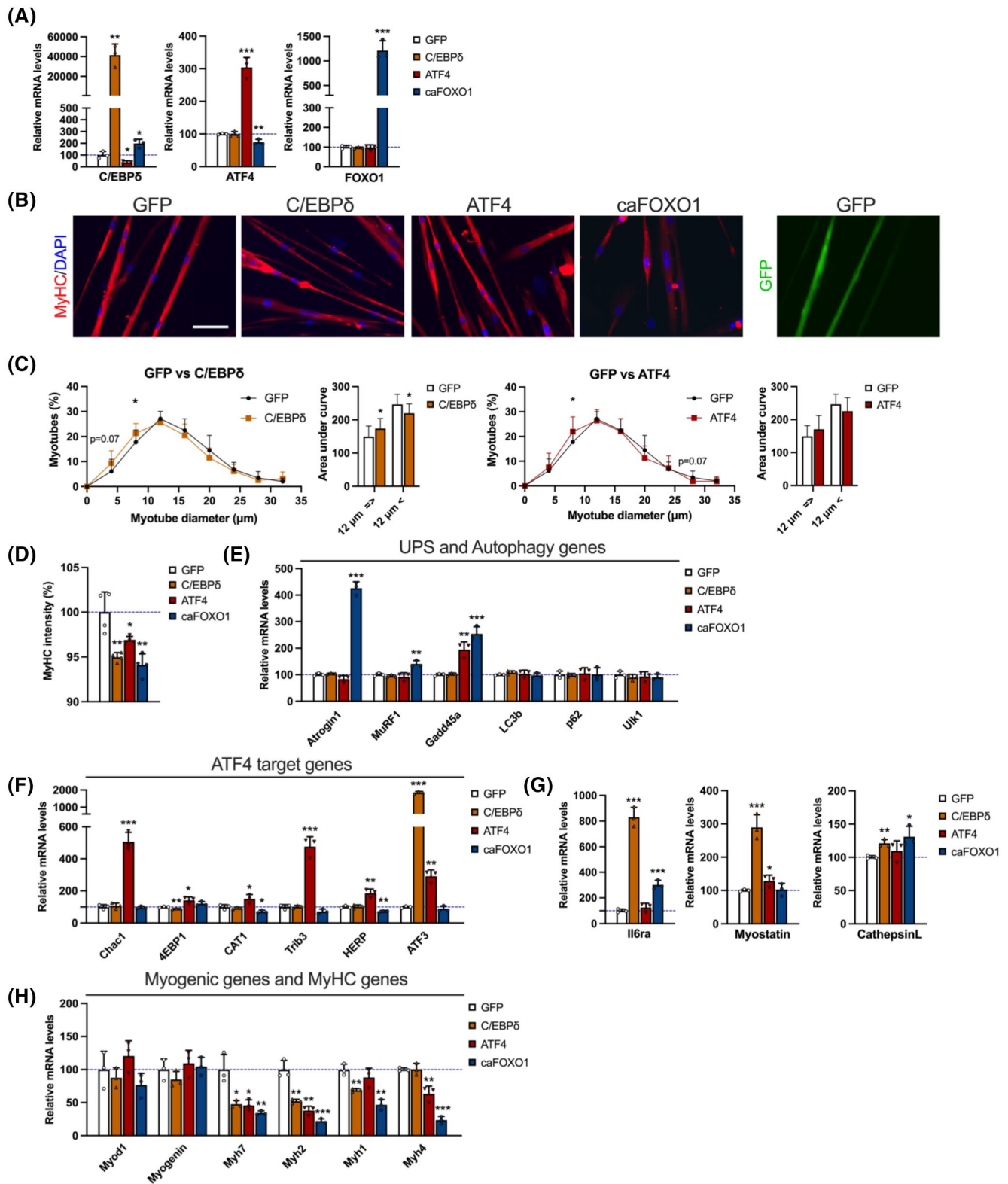


Figure 7B). Among these hub genes in FOXO-regulated DEGs were catabolic genes involved in protein ubiquitination [*Fbxo32* (Atrogin1), *Fbxl3*, *Fbxo9*, and *Trim63* (MuRF1)] (Cluster1) and autophagy [*Map1lc3b* (LC3b) and *Sqstm1* (p62)] (Cluster4), as well as ATF4, a transcription factor induced by ER stress and the unfolded

protein response<sup>62</sup> (Figure 7A,B). As expected, FOXO1 was also detected as a hub gene. Interestingly, among the top 20 putative hub genes, ATF4 is the only transcription factor except for FOXO1 (Figure 7B). Heatmap analysis of microarray data as used in Figures 3 and 4 demonstrated that 16 genes with direct edge to ATF4

including catabolic genes involved in autophagy [*Map1lc3b* (LC3b), *Sqstm1* (p62), and *Bnip3*] and mTORC1 inhibitor [*Ddit4* (*Redd1*)] as well as unfolded protein response genes [*Chac1*, *Ppp1r15a* (*Gadd34*), and *Edem1*]. These genes were under the control of FOXOs during fasting, namely upregulated in fasted WT muscle but not in fasted FOXO1,3a,4<sup>-/-</sup> muscle, indicating that ATF4 coordinately regulates the transcriptional program with FOXOs (Figure 7C). Importantly, ATF4 has been reported to induce muscle atrophy during fasting.<sup>21</sup> We found that ATF4 target genes, such as *Gadd45a*, *4EBP1*, *Redd1*, and *Chac1*, were upregulated in a FOXO-dependent manner during fasting (Figures 2D and 4D). Thus, we assessed whether FOXOs are required for the induction of ATF4 signaling during fasting. Transcript expression of *ATF4* and downstream target genes, including *Cat1*, *Trib3*, *Gadd34*, *Herp*, and *ATF3*,<sup>63-65</sup> significantly increased in fasted WT muscle but not in fasted FOXO1,3a,4<sup>-/-</sup> muscle (Figure 7D), suggesting that FOXOs induce ATF4 signaling during fasting in vivo.

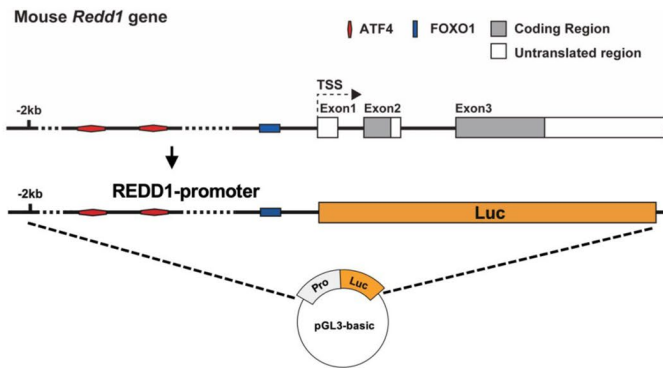
Based on the finding that ATF4 signaling was regulated by FOXOs in vivo, we checked whether ATF4 signaling was also regulated by FOXO1 in C2C12 myoblasts. ATF4 downstream target genes, including *Chac1*, *4EBP1*, *Trib3*, *Gadd34*, and *ATF3*, significantly increased in FOXO1-activated C2C12 myoblasts, supporting the existence of FOXO1-ATF4 signaling in C2C12 myoblasts (Figure S9C). Therefore, we examined whether loss of function using siATF4 had any effects on its target genes in C2C12 myoblasts expressing FOXO1-ER. As expected, the expression of ATF4 and its downstream target genes, including *Chac1*, *Gadd45a*, *Trib3*, *Gadd34*, and *ATF3*, were increased by FOXO1 activation (Figure 7E). When ATF4 was knocked down using siRNA, the induction of FOXO1-dependent *Chac1*, *Gadd45a*, *Trib3*, and *ATF3* transcripts were suppressed (Figure 7E), indicating that ATF4 functions downstream of FOXO1. These data further support the finding that ATF4 signaling was regulated by FOXOs.

### 3.11 | C/EBPδ or ATF4 overexpression is sufficient to induce primary myotube atrophy

A previous report has demonstrated that forced induction of C/EBPδ in C2C12 myoblasts increased protein degradation in differentiated myotubes.<sup>17</sup> We hypothesized that if C/EBPδ or ATF4 has a major role in muscle atrophy, overexpression of C/EBPδ or ATF4 in primary myotubes might be sufficient to induce myotube atrophy. The qRT-PCR analysis confirmed that *C/EBPδ* transcript expression dramatically increased in primary myotubes overexpressing C/EBPδ and in primary myotubes overexpressing caFOXO1, and *ATF4* transcript expression significantly increased in primary myotubes overexpressing ATF4 (Figure 8A). Immunofluorescent staining for MyHC showed that forced induction of C/EBPδ or ATF4 led to myotube atrophy as measured by the myotube diameter, MyHC intensity, and decreased *MyHC* gene expression, indicating that C/EBPδ or ATF4 is sufficient to induce muscle atrophy (Figure 8B–D,H). We analyzed markers of muscle atrophy by qRT-PCR and found that E3 ubiquitin ligase (*Atrogin1* and *MurF1*) and autophagy-related (*LC3b*, *p62*, and *Ulk1*) genes were not affected in primary myotubes overexpressing C/EBPδ or ATF4, suggesting that forced expression of C/EBPδ or ATF4 is not sufficient to induce the UPS and autophagy (Figure 8E). Instead, the expression of previously reported atrophy-related ATF4 target gene (*Gadd45a*, *4EBP1*, and *Trib3*)<sup>29,66,67</sup> and other ATF4 target genes (*Chac1*, *CAT1*, *HERP*, *ATF3*) transcript was significantly upregulated in primary myotubes overexpressing ATF4 (Figure 8E,F). We found that the expression of authentic C/EBPδ target gene (*Il6ra*)<sup>68</sup> and muscle atrophy-related gene (*Myostatin* and *CathepsinL*) transcript was upregulated in primary myotubes overexpressing C/EBPδ, suggesting that *Il6ra*, *Myostatin*, and *CathepsinL* are potential C/EBPδ target genes in skeletal muscle (Figure 8G). To further corroborate that forced induction of C/EBPδ leads to the myotube atrophy and these genes are potential C/EBPδ target

**FIGURE 8** C/EBPδ or ATF4 is sufficient to induce primary myotube atrophy. (A–H) Primary myoblasts isolated from the extensor digitorum longus (EDL) of C57BL6/J mice were transfected with the GFP, C/EBPδ, ATF4, or caFOXO1 expression vector, after which the cells were induced to differentiate into myotubes for 4 days. (A) Quantitative RT-PCR of C/EBPδ, ATF4, and FOXO1 in primary myotubes overexpressing GFP, C/EBPδ, ATF4, or caFOXO1 ( $n = 3$  sets of cells per group). (B) Primary myotubes overexpressing GFP, C/EBPδ, ATF4, or caFOXO1 were stained and visualized using immunofluorescence with an anti-myosin heavy chain (MyHC) antibody. Representative images were shown. Scale bar = 50 μm. Nuclei were stained with DAPI (blue). (C) Myotube distribution of different myotube diameter and area under curve (AUC) analysis of primary myotubes overexpressing GFP or C/EBPδ (left) and GFP or ATF4 (right)  $n = 16$  pictures (4 independent wells/condition). (D) Quantification of MyHC intensity in primary myotubes overexpressing GFP, C/EBPδ, ATF4, or caFOXO1 ( $n = 4$  sets of cells per group). (E–H) Quantitative RT-PCR of (E) muscle-specific ubiquitin ligases and autophagy genes, (F) ATF4 target genes, (G) C/EBPδ target and muscle atrophy-related genes, and (H) myogenic regulatory factor and myosin heavy chain genes in primary myotubes overexpressing GFP, C/EBPδ, ATF4, or caFOXO1 ( $n = 3$  sets of cells per group). All data were normalized with 36B4 expression and are shown as relative values to the control group (open bars). Values are mean ± SD. \* $p < .05$ , \*\* $p < .01$ , and \*\*\* $p < .001$  (Student's two-tailed unpaired  $t$ -test)

(A)



(B)

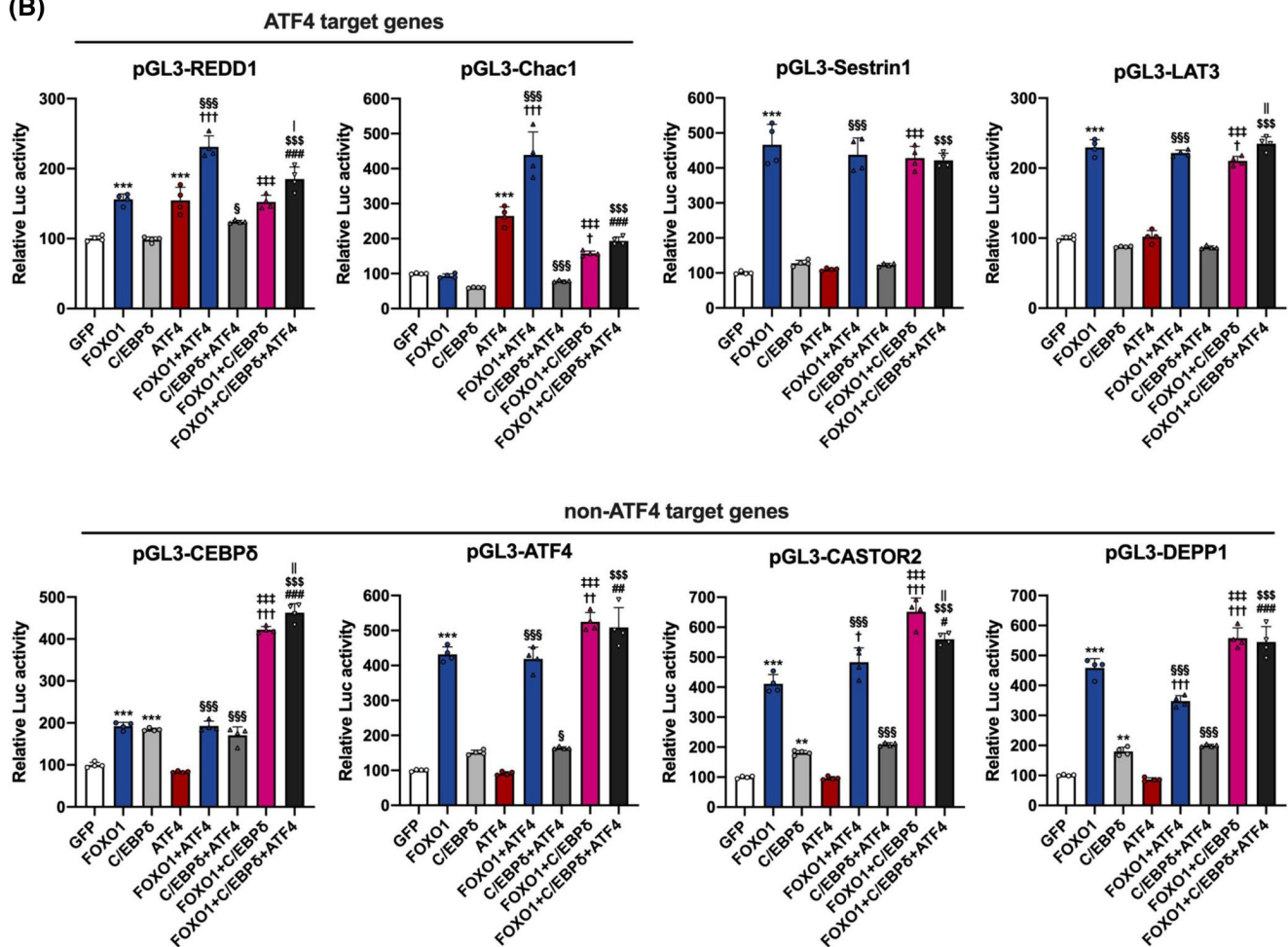


**FIGURE 9** FOXO1 coordinately enhances the promoter activity with C/EBP $\delta$  and ATF4. (A) Schematic illustration of cloning of mouse *Redd1* gene promoter [−1500 to +100 from transcription start site (TSS)] into luciferase reporter plasmid, in which the firefly *luciferase* gene is driven by the mouse *Redd1* promoter. *Redd1* gene promoter contains the conserved consensus FOXO1 binding site and two conserved ATF4 binding sites. (B) The effects of overexpression of FOXO1, C/EBP $\delta$ , and ATF4 on the novel FOXO1 target gene promoter activities were examined by co-transfection with reporter plasmids into HEK293T cells. Each construct includes the firefly *luciferase* gene driven by the mouse novel FOXO1 target gene promoter (C/EBP $\delta$ : −1500 to +25, ATF4: −1500 to +100, *Redd1*: −1500 to +100, *Sestrin1*: −1100 to +130, *Castor2*: −1900 to +100, *Chac1*: −2000 to +100, *Depp1*: −1500 to +100, and *Lat3*: −1000 to +90, from TSS). Firefly luciferase activities were normalized with Renilla luciferase activities as an internal control of transfection efficiency.  $n = 4$  sets of cells per group. Values are mean  $\pm$  SD. \*\* $p < .01$ , and \*\*\* $p < .001$  versus GFP alone, † $p < .05$ , †† $p < .01$ , and ††† $p < .001$  versus FOXO1 alone, †† $p < .01$ , and ††† $p < .001$  versus C/EBP $\delta$  alone, § $p < .05$ , and §§§ $p < .001$  versus ATF4 alone, # $p < .05$ , ## $p < .01$ , and ### $p < .001$  versus FOXO1 and ATF4, §§§ $p < .001$  versus C/EBP $\delta$  and ATF4, † $p < .05$  and †† $p < .01$  versus FOXO1 and C/EBP $\delta$  (One-way ANOVA followed by Tukey's *post hoc* test)

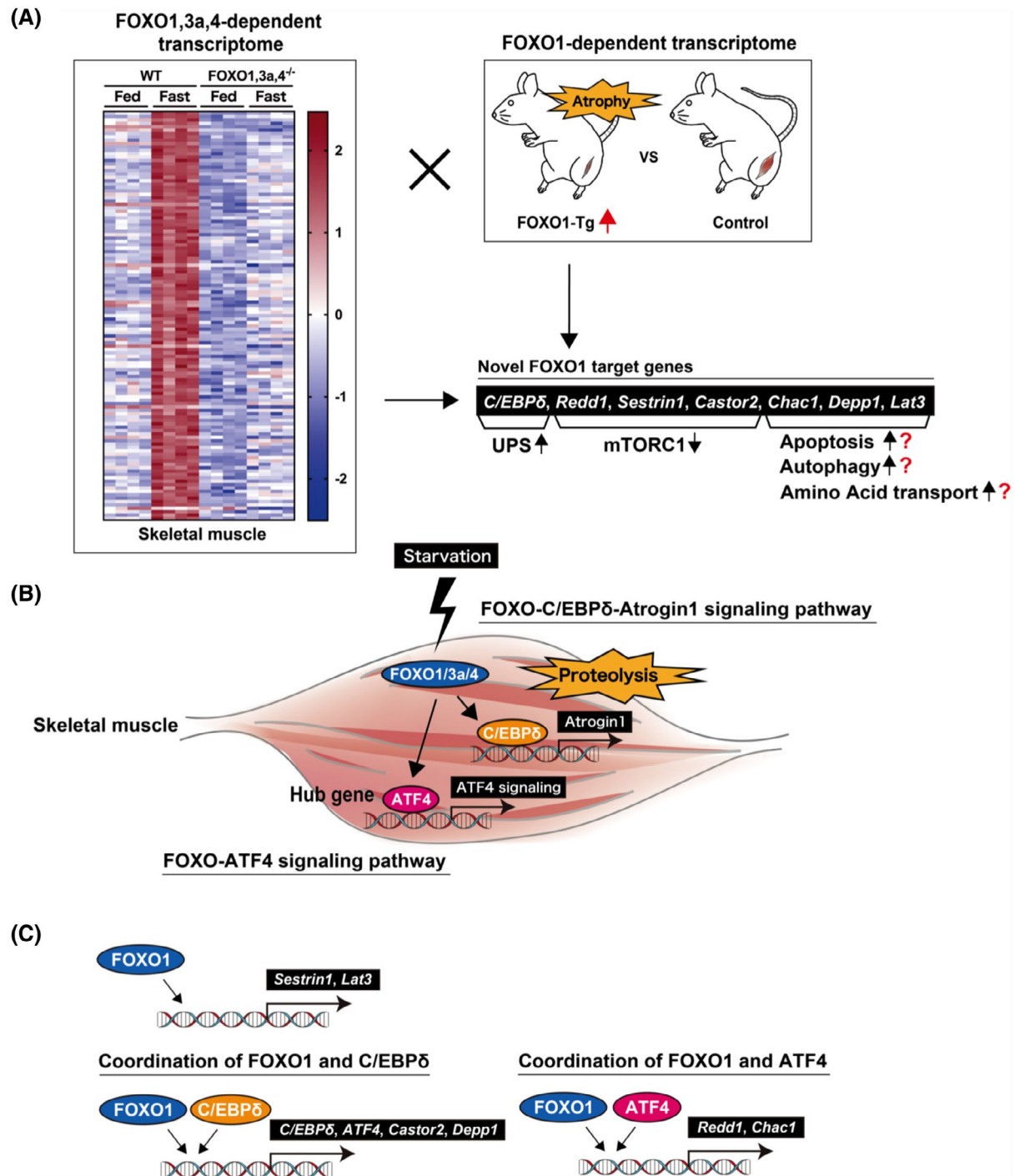


**FIGURE 10** Schematic summary of this study. (A) Schematic representation of novel FOXO1 target genes identification. The comparison between the transcriptome from FOXO1-Tg (gain-of-function model) mice and fasted FOXO1,3a,4<sup>-/-</sup> (loss-of-function model) mice identified several novel FOXO1-target genes in skeletal muscle, including *Redd1*, *Sestrin1*, *Castor2*, *Chac1*, *Depp1*, *Lat3*, as well as *C/EBPδ*. The heatmap is the same image as Figure 4B. (B) FOXO-C/EBPδ-Atrogin1 signaling pathway and FOXO-ATF4 signaling pathway. During starvation, FOXOs are responsible for the induction of *C/EBPδ* and *ATF4* in skeletal muscle. Concomitantly, FOXOs are responsible for the increased E3 ubiquitin ligase *Atrogin1* expression, protein ubiquitination, and *ATF4* target gene expression. In C2C12 myotubes, constitutively active FOXO1 increases *Atrogin1* and myofiber degradation via the *C/EBPδ* induction. (C) The transcriptional regulation mechanism by FOXO1. FOXO1 promotes the expression of target genes in cooperation with *C/EBPδ* and *ATF4*. There are at least three different mechanisms in the transcription regulation by FOXO1. (1) FOXO1 enhances *Sestrin1* and *Lat3* promoter activities. (2) FOXO1 and *C/EBPδ* coordinately enhance *C/EBPδ*, *ATF4*, *Castor2*, and *Depp1* promoter activities. (3) FOXO1 and *ATF4* coordinately enhance *Redd1* and *Chac1* promoter activities

genes in skeletal muscle, we generated C/EBP $\delta$  stable cell lines using a retrovirus. Stable C/EBP $\delta$  overexpression resulted in myotube atrophy and C/EBP $\delta$  target (*Il6ra*) and muscle atrophy-related (*Myostatin* and *CathepsinL*) gene transcripts were significantly upregulated in the primary myotubes stably overexpressing C/EBP $\delta$  (Figure S11A–F). Collectively, these results suggest that C/EBP $\delta$  or ATF4 is sufficient to induce muscle atrophy in primary myotubes.

### 3.12 | FOXO1 coordinately activates its target gene promoters with C/EBP $\delta$ and ATF4

Finally, we investigated whether novel FOXO1 target genes identified in this study could be direct transcriptional targets of FOXO1. FOXO1 has been reported to directly bind to two consensus FOXO1-binding sites [Daf-16 binding element (DBE): TT(G/A)TTTA(C/T)<sup>69</sup> and insulin response element: CAAAA(C/T)AA<sup>70</sup>] to regulate the promoter activity of its target genes. Therefore, we searched for two consensus FOXO1-binding sites in the putative promoter regions upstream of 2 kb from the transcription start sites and found at least 1 DBE or insulin response element in murine *C/EBP $\delta$* , *ATF4*, *Redd1*, *Sestrin1*, *Castor2*, *Chac1*, *Depp1*, and *Lat3* promoter regions, suggesting these genes are direct targets of FOXO1. We thus cloned the *C/EBP $\delta$* , *ATF4*, *Redd1*, *Sestrin1*, *Castor2*, *Chac1*, *Depp1*, and *Lat3* promoter into luciferase reporter plasmids, in which firefly *luciferase* genes were driven by the *C/EBP $\delta$* , *ATF4*, *Redd1*, *Sestrin1*, *Castor2*, *Chac1*, *Depp1*, and *Lat3* promoters, respectively (Figure 9A).

Since the above experiment showed that C/EBP $\delta$  and ATF4 are required for the induction of target genes by FOXO1 (Figures 6F,G,I and 7E), we assessed whether C/EBP $\delta$  and ATF4 coordinately regulate the novel FOXO1 target gene promoters by transiently transfecting the expression plasmids for FOXO1, C/EBP $\delta$ , and ATF4 into HEK293T cells. Consistent with previous reports that have demonstrated that *Redd1* and *Chac1* are direct targets of ATF4 and the consensus ATF4-binding sites [Amino acid response element: TGATGNAAN<sup>61</sup>] are conserved in *Redd1* and *Chac1* promoters (Figure S12A,C), *Redd1* and *Chac1* promoter activities were activated by ATF4 overexpression (Figure 9B). *Redd1* promoter activity was also activated by FOXO1 overexpression since *Redd1* promoter contains a conserved consensus FOXO1-binding site (DBE) (Figures 9B and S12B); however, *Chac1* promoter activity was not activated by FOXO1 (Figure 9B). Notably, *Redd1* and *Chac1* promoter activities were coordinately activated by FOXO1 and ATF4 (Figure 9B). *C/EBP $\delta$*  promoter activity was activated by C/EBP $\delta$

overexpression (Figure 9B), indicating that C/EBP $\delta$  promotes its own transcription as the autoregulation mechanism. Although C/EBP $\delta$  promoter activity was also activated by FOXO1 overexpression, it was further strongly activated by the coordination of FOXO1 and C/EBP $\delta$  (Figure 9B). *ATF4*, *Castor2*, and *Depp1* promoters were also coordinately activated by FOXO1 and C/EBP $\delta$  (Figure 9B). *Sestrin1* and *Lat3* promoter activities were only activated by FOXO1 (Figure 9B).

Taken together, the above data indicate that FOXO1 activates these target gene promoters in cooperation with C/EBP $\delta$  and ATF4, and there are at least three different mechanisms of transcription regulation by FOXO1 (Figure S13A–C).

## 4 | CONCLUSION

The key findings of this study are as follows: (1) We identified *C/EBP $\delta$* , *ATF4*, *Redd1*, *Sestrin1*, *Castor2*, *Chac1*, *Depp1*, and *Lat3* as novel FOXO1 target genes in skeletal muscle by comparing the gene expression profiles from FOXO1-Tg (gain-of-function model) mice with fasted FOXO1,3a,4<sup>-/-</sup> (loss-of-function model) mice in vivo (Figure 10A). (2) FOXO–C/EBP $\delta$  signaling pathway emerged as a novel proteolytic pathway that links FOXO1 and UPS-mediated proteolysis, and FOXO1/ATF4 signaling is essential for the induction of ATF4 target genes in skeletal muscle (Figure 10B). (3) We found FOXO1 coordinately activates its target gene promoters with C/EBP $\delta$  and ATF4 (Figure 10C). It is important to understand the molecular mechanism and signaling pathway underlying FOXO-induced muscle atrophy since FOXOs are central regulators of muscle atrophy, and deletion of FOXOs prevents excessive muscle loss in a diverse range of detrimental catabolic conditions, including starvation and denervation,<sup>10,11</sup> hindlimb suspension,<sup>12</sup> immobilization,<sup>13</sup> cancer and sepsis cachexia,<sup>71</sup> diabetes mellitus,<sup>14</sup> and chronic kidney disease.<sup>15</sup> Thus, by identifying the novel FOXO1 target genes in vivo, we obtained important clues for understanding the physiology/pathophysiology of FOXO1, a master regulator of skeletal muscle atrophy.

## ACKNOWLEDGMENTS

We thank Dr. Ayaka Ito (Nagoya University) for her advice on statistical analysis, and Dr. Yusuke Ono (Kumamoto University) for discussion. Microarray data analysis was, in part, performed at the Medical Research Support Center, Graduate School of Medicine, Kyoto University. This study is supported by grants-in-aid for scientific research (KAKENHI) from the Japanese Ministry of Education, Culture, Sports, Science, and Technology (MEXT, Tokyo).

This study is also supported by The Fuji Foundation for Protein Research and by The Tojuro Iijima Foundation for Food Science and Technology. The funders had no role in study design, data collection and analysis, the decision to publish, and preparation of the manuscript.

## DISCLOSURES

The authors declare that they have no conflicts of interest with the contents of this article.

## AUTHOR CONTRIBUTIONS

Mamoru Oyabu, Yukino Hatazawa, Shinji Miura, and Yasutomi Kamei conceived and designed the experiments. Mamoru Oyabu, Kaho Takigawa, Sako Mizutani, Yukino Hatazawa, Fujita Fujita, Yuto Ohira, Takumi Sugimoto, and Kengo Ishihara performed the experiments. Mamoru Oyabu, Osamu Suzuki, Takumi Suganami, Yoshihiro Ogawa, Shinji Miura, and Yasutomi Kamei analyzed the data. Osamu Suzuki, Kyoichiro Tsuchiya, Takayoshi Suganami, Yoshihiro Ogawa, Kengo Ishihara, Shinji Miura, and Yasutomi Kamei contributed reagents and materials/analysis tools. Mamoru Oyabu, Fujita Fujita, and Yasutomi Kamei wrote the article.

## ORCID

Osamu Suzuki  <https://orcid.org/0000-0002-9003-7282>  
 Takayoshi Suganami  <https://orcid.org/0000-0002-1918-0465>  
 Yoshihiro Ogawa  <https://orcid.org/0000-0002-0834-2836>  
 Kengo Ishihara  <https://orcid.org/0000-0001-9374-5033>  
 Shinji Miura  <https://orcid.org/0000-0001-8806-9763>  
 Yasutomi Kamei  <https://orcid.org/0000-0003-2778-926X>

## REFERENCES

- Zhou X, Wang JL, Lu J, et al. Reversal of cancer cachexia and muscle wasting by ActRIIB antagonism leads to prolonged survival. *Cell*. 2010;142:531-543.
- Martin L, Birdsall L, Macdonald N, et al. Cancer cachexia in the age of obesity: skeletal muscle depletion is a powerful prognostic factor, independent of body mass index. *J Clin Oncol*. 2013;31:1539-1547.
- Bodine SC, Latres E, Baumhueter S, et al. Identification of ubiquitin ligases required for skeletal muscle atrophy. *Science*. 2001;294:1704-1708.
- Sandri M, Sandri C, Gilbert A, et al. Foxo transcription factors induce the atrophy-related ubiquitin ligase atrogin-1 and cause skeletal muscle atrophy. *Cell*. 2004;117:399-412.
- Schiaffino S, Dyar KA, Ciciliot S, Blaauw B, Sandri M. Mechanisms regulating skeletal muscle growth and atrophy. *FEBS J*. 2013;280:4294-4314.
- Accili D, Arden KC. FoxOs at the crossroads of cellular metabolism, differentiation, and transformation. *Cell*. 2004;117:421-426.
- Waddell DS, Baehr LM, van den Brandt J, et al. The glucocorticoid receptor and FOXO1 synergistically activate the skeletal muscle atrophy-associated MuRF1 gene. *American journal of physiology. Endocrinol Metab*. 2008;295:E785-E797.
- Zhao J, Brault JJ, Schild A, et al. FoxO3 coordinately activates protein degradation by the autophagic/lysosomal and proteasomal pathways in atrophying muscle cells. *Cell Metab*. 2007;6:472-483.
- Mammucari C, Milan G, Romanello V, et al. FoxO3 controls autophagy in skeletal muscle in vivo. *Cell Metab*. 2007;6:458-471.
- Milan G, Romanello V, Pescatore F, et al. Regulation of autophagy and the ubiquitin-proteasome system by the FoxO transcriptional network during muscle atrophy. *Nat Commun*. 2015;6:6670.
- Tang H, Inoki K, Lee M, et al. mTORC1 promotes denervation-induced muscle atrophy through a mechanism involving the activation of FoxO and E3 ubiquitin ligases. *Sci Signal*. 2014;7:ra18.
- Brocca L, Toniolo L, Reggiani C, Bottinelli R, Sandri M, Pellegrino MA. FoxO-dependent atrogenes vary among catabolic conditions and play a key role in muscle atrophy induced by hindlimb suspension. *J Physiol*. 2017;595:1143-1158.
- Segales J, Perdiguero E, Serrano AL, et al. Sestrin prevents atrophy of disused and aging muscles by integrating anabolic and catabolic signals. *Nat Commun*. 2020;11:189.
- O'Neill BT, Bhardwaj G, Penniman CM, et al. FoxO transcription factors are critical regulators of diabetes-related muscle atrophy. *Diabetes*. 2019;68:556-570.
- Xu J, Li R, Workeneh B, Dong Y, Wang X, Hu Z. Transcription factor FoxO1, the dominant mediator of muscle wasting in chronic kidney disease, is inhibited by microRNA-486. *Kidney Int*. 2012;82:401-411.
- Silva KA, Dong J, Dong Y, et al. Inhibition of Stat3 activation suppresses caspase-3 and the ubiquitin-proteasome system, leading to preservation of muscle mass in cancer cachexia. *J Biol Chem*. 2015;290:11177-11187.
- Zhang L, Pan J, Dong Y, et al. Stat3 activation links a C/EBPdelta to myostatin pathway to stimulate loss of muscle mass. *Cell Metab*. 2013;18:368-379.
- Sekine K, Chen YR, Kojima N, Ogata K, Fukamizu A, Miyajima A. Foxo1 links insulin signaling to C/EBPalpha and regulates gluconeogenesis during liver development. *EMBO J*. 2007;26:3607-3615.
- Ito Y, Daitoku H, Fukamizu A. Foxo1 increases pro-inflammatory gene expression by inducing C/EBPbeta in TNF-alpha-treated adipocytes. *Biochem Biophys Res Commun*. 2009;378:290-295.
- Daitoku H, Sakamaki J, Fukamizu A. Regulation of FoxO transcription factors by acetylation and protein-protein interactions. *Biochim Biophys Acta*. 2011;1813:1954-1960.
- Ebert SM, Monteys AM, Fox DK, et al. The transcription factor ATF4 promotes skeletal myofiber atrophy during fasting. *Mol Endocrinol*. 2010;24:790-799.
- Ebert SM, Bullard SA, Basisty N, et al. Activating transcription factor 4 (ATF4) promotes skeletal muscle atrophy by forming a heterodimer with the transcriptional regulator C/EBPbeta. *J Biol Chem*. 2020;295:2787-2803.
- Kamei Y, Miura S, Suzuki M, et al. Skeletal muscle FOXO1 (FKHR) transgenic mice have less skeletal muscle mass, down-regulated Type I (slow twitch/red muscle) fiber genes, and impaired glycemic control. *J Biol Chem*. 2004;279:41114-41123.
- Furuyama T, Kitayama K, Yamashita H, Mori N. Forkhead transcription factor FOXO1 (FKHR)-dependent induction of PDK4

- gene expression in skeletal muscle during energy deprivation. *Biochem J.* 2003;375:365-371.
25. Yamazaki Y, Kamei Y, Sugita S, et al. The cathepsin L gene is a direct target of FOXO1 in skeletal muscle. *Biochem J.* 2010;427:171-178.
  26. Demontis F, Perrimon N. FOXO/4E-BP signaling in Drosophila muscles regulates organism-wide proteostasis during aging. *Cell.* 2010;143:813-825.
  27. Pin F, Novinger LJ, Huot JR, et al. PDK4 drives metabolic alterations and muscle atrophy in cancer cachexia. *FASEB J.* 2019;33:7778-7790.
  28. Deval C, Mordier S, Obled C, et al. Identification of cathepsin L as a differentially expressed message associated with skeletal muscle wasting. *Biochem J.* 2001;360:143-150.
  29. Ebert SM, Dyle MC, Kunkel SD, et al. Stress-induced skeletal muscle Gadd45a expression reprograms myonuclei and causes muscle atrophy. *J Biol Chem.* 2012;287:27290-27301.
  30. Bodine SC, Stitt TN, Gonzalez M, et al. Akt/mTOR pathway is a crucial regulator of skeletal muscle hypertrophy and can prevent muscle atrophy in vivo. *Nat Cell Biol.* 2001;3:1014-1019.
  31. O'Neill BT, Lee KY, Klaus K, et al. Insulin and IGF-1 receptors regulate FoxO-mediated signaling in muscle proteostasis. *J Clin Invest.* 2016;126:3433-3446.
  32. Castrillon DH, Miao L, Kollipara R, Horner JW, DePinho RA. Suppression of ovarian follicle activation in mice by the transcription factor Foxo3a. *Science (New York, NY).* 2003;301:215-218.
  33. Paik JH, Kollipara R, Chu G, et al. FoxOs are lineage-restricted redundant tumor suppressors and regulate endothelial cell homeostasis. *Cell.* 2007;128:309-323.
  34. Ishihara K, Taniguchi H. Fat max as an index of aerobic exercise performance in mice during uphill running. *PLoS One.* 2018;13:e0193470.
  35. Taniguchi H, Akiyama N, Ishihara K. Hepatic fat content is associated with fasting-induced fibroblast growth factor 21 secretion in mice fed soy proteins. *J Nutr Sci Vitaminol (Tokyo).* 2019;65:515-525.
  36. da Huang W, Sherman BT, Lempicki RA. Systematic and integrative analysis of large gene lists using DAVID bioinformatics resources. *Nat Protoc.* 2009;4:44-57.
  37. Szklarczyk D, Gable AL, Lyon D, et al. STRING v11: protein-protein association networks with increased coverage, supporting functional discovery in genome-wide experimental datasets. *Nucleic Acids Res.* 2019;47:D607-D613.
  38. Shannon P, Markiel A, Ozier O, et al. Cytoscape: a software environment for integrated models of biomolecular interaction networks. *Genome Res.* 2003;13:2498-2504.
  39. Bastie CC, Nahle Z, McLoughlin T, et al. FoxO1 stimulates fatty acid uptake and oxidation in muscle cells through CD36-dependent and -independent mechanisms. *J Biol Chem.* 2005;280:14222-14229.
  40. Schmidt EK, Clavarino G, Ceppi M, Pierre P. SUnSET, a non-radioactive method to monitor protein synthesis. *Nat Methods.* 2009;6:275-277.
  41. Iwasaki Y, Suganami T, Hachiya R, et al. Activating transcription factor 4 links metabolic stress to interleukin-6 expression in macrophages. *Diabetes.* 2014;63:152-161.
  42. Lecker SH, Jagoe RT, Gilbert A, et al. Multiple types of skeletal muscle atrophy involve a common program of changes in gene expression. *FASEB J.* 2004;18:39-51.
  43. Sackey JM, Hyatt JP, Raffaello A, et al. Rapid disuse and denervation atrophy involve transcriptional changes similar to those of muscle wasting during systemic diseases. *FASEB J.* 2007;21:140-155.
  44. Sanchez AM, Candau RB, Bernardi H. FoxO transcription factors: their roles in the maintenance of skeletal muscle homeostasis. *Cell Mol Life Sci.* 2014;71:1657-1671.
  45. Shimizu N, Yoshikawa N, Ito N, et al. Crosstalk between glucocorticoid receptor and nutritional sensor mTOR in skeletal muscle. *Cell Metab.* 2011;13:170-182.
  46. Kuo T, Harris CA, Wang JC. Metabolic functions of glucocorticoid receptor in skeletal muscle. *Mol Cell Endocrinol.* 2013;380:79-88.
  47. Hirata Y, Nomura K, Senga Y, et al. Hyperglycemia induces skeletal muscle atrophy via a WWP1/KLF15 axis. *JCI Insight.* 2019;4.
  48. Niu M, Li L, Su Z, et al. An integrative transcriptome study reveals Ddit4/Redd1 as a key regulator of cancer cachexia in rodent models. *Cell Death Dis.* 2021;12:652.
  49. Wang H, Kubica N, Ellisen LW, Jefferson LS, Kimball SR. Dexamethasone represses signaling through the mammalian target of rapamycin in muscle cells by enhancing expression of REDD1. *J Biol Chem.* 2006;281:39128-39134.
  50. Chantranupong L, Wolfson RL, Orozco JM, et al. The Sestrins interact with GATOR2 to negatively regulate the amino-acid-sensing pathway upstream of mTORC1. *Cell Rep.* 2014;9:1-8.
  51. Chantranupong L, Scaria SM, Saxton RA, et al. The CASTOR proteins are arginine sensors for the mTORC1 pathway. *Cell.* 2016;165:153-164.
  52. Mungrue IN, Pagnon J, Kohannim O, Gargalovic PS, Lusis AJ. CHAC1/MGC4504 is a novel proapoptotic component of the unfolded protein response, downstream of the ATF4-ATF3-CHOP cascade. *J Immunol.* 2009;182:466-476.
  53. Salcher S, Hermann M, Kiechl-Kohlendorfer U, Ausserlechner MJ, Obexer P. C10ORF10/DEPP-mediated ROS accumulation is a critical modulator of FOXO3-induced autophagy. *Mol Cancer.* 2017;16:95.
  54. Fukuhara D, Kanai Y, Chairoungdua A, et al. Protein characterization of NA+-independent system L amino acid transporter 3 in mice: a potential role in supply of branched-chain amino acids under nutrient starvation. *Am J Pathol.* 2007;170:888-898.
  55. Xu D, Shimkus KL, Lacko HA, Kutzler L, Jefferson LS, Kimball SR. Evidence for a role for Sestrin1 in mediating leucine-induced activation of mTORC1 in skeletal muscle. *Am J Physiol Endocrinol Metab.* 2019;316:E817-E828.
  56. Chen CC, Jeon SM, Bhaskar PT, et al. FoxOs inhibit mTORC1 and activate Akt by inducing the expression of Sestrin3 and Rictor. *Dev Cell.* 2010;18:592-604.
  57. Matsuzaki H, Daitoku H, Hatta M, Tanaka K, Fukamizu A. Insulin-induced phosphorylation of FKHR (Foxo1) targets to proteasomal degradation. *Proc Natl Acad Sci USA.* 2003;100:11285-11290.
  58. Batista TM, Garcia-Martin R, Cai W, et al. Multi-dimensional transcriptional remodeling by physiological insulin in vivo. *Cell Rep.* 2019;26:3429-3443.e3423.
  59. Yang H, Mammen J, Wei W, et al. Expression and activity of C/EBPbeta and delta are upregulated by dexamethasone in skeletal muscle. *J Cell Physiol.* 2005;204:219-226.

60. Allen DL, Cleary AS, Hanson AM, Lindsay SF, Reed JM. CCAAT/enhancer binding protein-delta expression is increased in fast skeletal muscle by food deprivation and regulates myostatin transcription in vitro. *Am J Physiol Regul Integr Comp Physiol*. 2010;299:R1592-R1601.
61. Pakos-Zebrucka K, Koryga I, Mnich K, Ljujic M, Samali A, Gorman AM. The integrated stress response. *EMBO Rep*. 2016;17:1374-1395.
62. Bohnert KR, McMillan JD, Kumar A. Emerging roles of ER stress and unfolded protein response pathways in skeletal muscle health and disease. *J Cell Physiol*. 2018;233:67-78.
63. Kilberg MS, Shan J, Su N. ATF4-dependent transcription mediates signaling of amino acid limitation. *Trends Endocrinol Metab*. 2009;20:436-443.
64. Lopez AB, Wang C, Huang CC, et al. A feedback transcriptional mechanism controls the level of the arginine/lysine transporter cat-1 during amino acid starvation. *Biochem J*. 2007;402:163-173.
65. Ma Y, Hendershot LM. Delineation of a negative feedback regulatory loop that controls protein translation during endoplasmic reticulum stress. *J Biol Chem*. 2003;278:34864-34873.
66. Choi RH, McConahay A, Silvestre JG, Moriscot AS, Carson JA, Koh HJ. TRB3 regulates skeletal muscle mass in food deprivation-induced atrophy. *FASEB J*. 2019;33:5654-5666.
67. Tsai S, Sitzmann JM, Dastidar SG, et al. Muscle-specific 4E-BP1 signaling activation improves metabolic parameters during aging and obesity. *J Clin Investig*. 2015;125:2952-2964.
68. Balamurugan K, Mendoza-Villanueva D, Sharan S, et al. C/EBPdelta links IL-6 and HIF-1 signaling to promote breast cancer stem cell-associated phenotypes. *Oncogene*. 2019;38:3765-3780.
69. Furuyama T, Nakazawa T, Nakano I, Mori N. Identification of the differential distribution patterns of mRNAs and consensus binding sequences for mouse DAF-16 homologues. *Biochem J*. 2000;349:629-634.
70. Guo S, Rena G, Cichy S, He X, Cohen P, Unterman T. Phosphorylation of serine 256 by protein kinase B disrupts transactivation by FKHR and mediates effects of insulin on insulin-like growth factor-binding protein-1 promoter activity through a conserved insulin response sequence. *J Biol Chem*. 1999;274:17184-17192.
71. Reed SA, Sandesara PB, Senf SM, Judge AR. Inhibition of FoxO transcriptional activity prevents muscle fiber atrophy during cachexia and induces hypertrophy. *FASEB J*. 2012;26:987-1000.

## SUPPORTING INFORMATION

Additional supporting information may be found in the online version of the article at the publisher's website.

**How to cite this article:** Oyabu M, Takigawa K, Mizutani S, et al. FOXO1 cooperates with C/EBP $\delta$  and ATF4 to regulate skeletal muscle atrophy transcriptional program during fasting. *FASEB J*. 2022;36:e22152. doi:[10.1096/fj.202101385RR](https://doi.org/10.1096/fj.202101385RR)